CHAPTER 6

Effects of Transport Limitations on Rates of Solid-Catalyzed Reactions

6.1 | Introduction

To most effectively utilize a catalyst in a commercial operation, the reaction rate is often adjusted to be approximately the same order of magnitude as the rates of transport phenomena. If a catalyst particle in an industrial reactor were operating with an extremely low turnover frequency, diffusive transport of chemicals to and from the catalyst surface would have no effect on the measured rates. While this "reaction-limited" situation is ideal for the determination of intrinsic reaction kinetics, it is clearly an inefficient way to run a process. Likewise, if a catalyst particle were operating under conditions that normally give an extremely high turnover frequency, the overall observed reaction rate is lowered by the inadequate transport of reactants to the catalyst surface. A balance between reaction rate and transport phenomena is frequently considered the most effective means of operating a catalytic reaction. For typical process variables in industrial reactors, this balance is achieved by adjusting reaction conditions to give a rate on the order of 1 μmol/(cm^3-s) [P. B. Weisz, *CHEMTECH*, (July 1982) 424]. This reaction rate translates into a turnover frequency of about 1 s^{-1} for many catalysts (R. L. Burwell, Jr. and M. Boudart, in "Investigations of Rates and Mechanisms of Reactions," Part 1, Ch. 12, E. S. Lewis, Ed., John Wiley, New York, 1974).

Figure 6.1.1 depicts the concentration profile of a reactant in the vicinity of a catalyst particle. In region 1, the reactant diffuses through the stagnant boundary layer surrounding the particle. Since the transport phenomena in this region occur outside the catalyst particle, they are commonly referred to as *external,* or

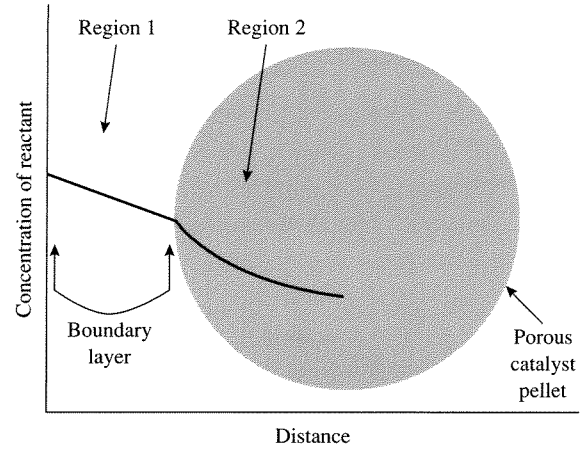

Figure 6.1.1 |
Concentration profile of a reacting species in the vicinity of a porous catalyst particle. Distances are not to scale.

interphase, transport effects. In region 2, the reactant diffuses into the pores of the particle, and transport phenomena in this region are called *internal*, or *intraphase*, transport effects. Both external and internal transport effects may be important in a catalytic reaction and are discussed separately in the following sections. In addition to mass transfer effects, heat transfer throughout the catalyst particle and the stagnant boundary layer can dramatically affect observed reaction rates.

6.2 | External Transport Effects

For a solid-catalyzed reaction to take place, a reactant in the fluid phase must first diffuse through the stagnant boundary layer surrounding the catalyst particle. This mode of transport is described (in one spatial dimension) by the Stefan-Maxwell equations (see Appendix C for details):

$$\nabla X_i = \sum_{\substack{j=1 \\ j \neq i}}^{n} \frac{1}{C D_{ij}} (X_i N_j - X_j N_i) \tag{6.2.1}$$

where X_i is the mole fraction of component i, C is the total concentration, N_i is the flux of component i, and D_{ij} is the diffusivity of component i in j. The following relationship for diffusion of A in a two component mixture at constant pressure (constant total concentration) can be obtained from simplifying the Stefan-Maxwell equations:

$$\nabla C_A = \frac{1}{D_{AB}} (X_A N_B - X_B N_A) \tag{6.2.2}$$

Since there are only two components in the mixture, $X_B = 1 - X_A$ and the above expression reduces to:

$$\nabla C_A = \frac{1}{D_{AB}}[X_A(N_A + N_B) - N_A] \tag{6.2.3}$$

Equimolar counterdiffusion ($N_A = -N_B$) can often be assumed and further simplification is thus possible to give:

$$\nabla C_A = \frac{-N_A}{D_{AB}} \tag{6.2.4}$$

The same equation can also be derived by assuming that concentrations are so dilute that $X_A(N_A + N_B)$ can be neglected. Equation (6.2.3) is known as Fick's First Law and can be written as:

$$N_A = -D_{AB}\nabla C_A \qquad \text{(equimolar counterdiffusion and/or dilute concentration of } A\text{)} \tag{6.2.5}$$

The diffusivities of gases and liquids typically have magnitudes that are 10^{-1} and 10^{-5} cm^2 s^{-1}, respectively. The diffusivity of gases is proportional to $T^{1.5}$ and inversely proportional to P, whereas, the diffusivity of liquids is proportional to T and inversely proportional to viscosity $\overline{\mu}$ (may strongly depend on T).

To obtain the flux of reactant A through the stagnant boundary layer surrounding a catalyst particle, one solves Equation (6.2.5) with the appropriate boundary conditions. If the thickness of the boundary layer $\bar{\delta}$ is small compared to the radius of curvature of the catalyst particle, then the problem can be solved in one dimension as depicted in Figure 6.2.1. In this case, Fick's Law reduces to:

$$N_{Ax} = -D_{AB}\frac{dC_A}{dx} \tag{6.2.6}$$

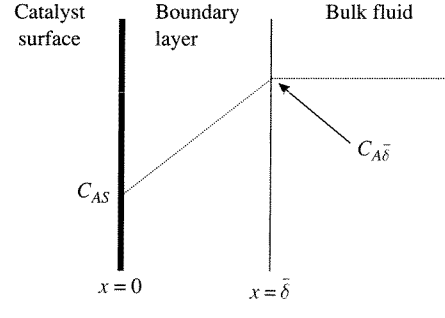

Figure 6.2.1 |
Concentration profile of reactant A in the vicinity of a catalyst particle.

Since the flux of A must be constant through the stagnant film (conservation of mass), the derivative of the flux with respect to distance in the film must vanish:

$$\frac{dN_{Ax}}{dx} = 0 \tag{6.2.7}$$

Differentiating Equation (6.2.6) (assuming constant diffusivity) and combining with Equation (6.2.7), yields the following differential equation that describes diffusion through a stagnant film:

$$\frac{d^2C_A}{dx^2} = 0 \tag{6.2.8}$$

with boundary conditions:

$$C_A = C_{AS} \qquad \text{at } x = 0 \tag{6.2.9}$$

$$C_A = C_{A\bar{\delta}} \qquad \text{at } x = \bar{\delta} \tag{6.2.10}$$

The solution of Equation (6.2.8) results in a linear concentration profile through the boundary layer:

$$C_A = C_{AS} + (C_{A\bar{\delta}} - C_{AS})\frac{x}{\bar{\delta}} \tag{6.2.11}$$

and the molar flux of A through the film is simply:

$$N_{Ax} = \frac{-D_{AB}}{\bar{\delta}}(C_{A\bar{\delta}} - C_{AS}) \tag{6.2.12}$$

Although diffusion of reacting species can be written in terms of the diffusivity and boundary layer thickness, the magnitude of $\bar{\delta}$ is unknown. Therefore, the mass-transfer coefficient is normally used. That is, the average molar flux from the bulk fluid to the solid surface is ($-x$ direction in Figure 6.2.1)

$$N_A = \bar{k}_c(C_{A\bar{\delta}} - C_{AS}) \tag{6.2.13}$$

where $\bar{k}_c$ is the mass transfer coefficient over the surface area of the particle. The mass transfer coefficient is obtained from correlations and is a function of the fluid velocity past the particle. If the fluid is assumed to be well mixed, the concentration of A at the edge of the stagnant boundary layer is equivalent to that in the bulk fluid, C_{AB}, and Equation (6.2.13) can therefore be written as:

$$N_A = \bar{k}_c(C_{AB} - C_{AS}) \tag{6.2.14}$$

At steady-state, the flux of A equals the rate of reaction thus preventing accumulation or depletion. For a simple first-order reaction, the kinetics depend on the surface rate constant, k_S, and the concentration of A at the surface:

$$\mathrm{r} = k_S C_{AS} = \bar{k}_c\left(C_{AB} - C_{AS}\right) \tag{6.2.15}$$

Solving for C_{AS} yields:

$$C_{AS} = \frac{\bar{k}_c C_{AB}}{k_S + \bar{k}_c} \tag{6.2.16}$$

Substitution of the above expression for C_{AS} into Equation (6.2.15) gives a rate expression in terms of the measurable quantity, C_{AB}, the reactant concentration in the bulk fluid:

$$\mathrm{r} = \frac{k_S \bar{k}_c}{k_S + \bar{k}_c} C_{AB} = \frac{C_{AB}}{\frac{1}{k_S} + \frac{1}{\bar{k}_c}} \tag{6.2.17}$$

An overall, observed rate constant can be defined in terms of k_S and $\bar{k}_c$ as:

$$\frac{1}{k_{\text{obs}}} = \left(\frac{1}{k_S}\right) + \left(\frac{1}{\bar{k}_c}\right) \tag{6.2.18}$$

so that the rate expressed in terms of observable quantities can be written as:

$$\mathrm{r}_{\text{obs}} = k_{\text{obs}} C_{AB} \tag{6.2.19}$$

For rate laws that are noninteger or complex functions of the concentration, C_{AS} is found by trial and error solution of the flux expression equated to the reaction rate. The influence of diffusional resistance on the observed reaction rate is especially apparent for a very fast surface reaction. For that case, the surface concentration of reactant is very small compared to its concentration in the bulk fluid. The observed rate is then written according to Equation (6.2.15), but ignoring C_{AS}:

$$\mathrm{r}_{\text{obs}} = \bar{k}_c C_{AB} \tag{6.2.20}$$

The observed rate will appear to be first-order with respect to the bulk reactant concentration, regardless of the intrinsic rate expression applicable to the surface reaction. This is a clear example of how external diffusion can mask the intrinsic kinetics of a catalytic reaction. In a catalytic reactor operating under mass transfer limitations, the conversion at the reactor outlet can be calculated by incorporating Equation (6.2.20) into the appropriate reactor model.

Solution of a reactor problem in the mass transfer limit requires an estimation of the appropriate mass transfer coefficient. Fortunately, mass transfer correlations have been developed to aid the determination of mass transfer coefficients. For example, the Sherwood number, Sh, relates the mass transfer coefficient of a species A to its diffusivity and the radius of a catalyst particle, R_p:

$$Sh = \frac{\bar{k}_c (2R_p)}{D_{AB}} \tag{6.2.21}$$

For flow around spherical particles, the Sherwood number is correlated to the Schmidt number, Sc, and the Reynolds number, Re:

$$Sh = 2 + 0.6 Re^{1/2} Sc^{1/3} \tag{6.2.22}$$

$$Sc = \frac{\bar{\mu}}{\rho D_{AB}} \tag{6.2.23}$$

$$Re = \frac{u\rho(2R_p)}{\bar{\mu}} \tag{6.2.24}$$

where $\bar{\mu}$ is the viscosity (kg m^{-1} s^{-1}), ρ is the fluid density (kg m^{-3}), and u is the linear fluid velocity (m s^{-1}). However, most mass-transfer results are correlated in terms of Colburn J factors:

$$J = \frac{Sh}{Sc^{1/3}Re} \tag{6.2.25}$$

that are plotted as a function of the Reynolds number. These J factor plots are available in most textbooks on mass transfer. If one can estimate the fluid density, velocity, viscosity, diffusivity, and catalyst particle size, then a reasonable approximation of the mass-transfer coefficient can be found.

It is instructive to examine the effects of easily adjustable process variables on the mass-transfer coefficient. Combining Equations (6.2.21–6.2.24) gives the functional dependence of the mass-transfer coefficient:

$$\bar{k}_c \propto \frac{D_{AB}Sh}{R_p} \propto \frac{D_{AB}}{R_p} Re^{1/2} Sc^{1/3} \propto \frac{D_{AB}}{R_p}\left(\frac{R_p u\rho}{\bar{\mu}}\right)^{1/2}\left(\frac{\bar{\mu}}{\rho D_{AB}}\right)^{1/3} \propto \frac{\left(D_{AB}\right)^{2/3} u^{1/2}\rho^{1/6}}{\left(R_p\right)^{1/2}\left(\bar{\mu}\right)^{1/6}}$$

or

$$\bar{k}_c \propto \frac{\left(D_{AB}\right)^{2/3} u^{1/2}\rho^{1/6}}{\left(R_p\right)^{1/2}\left(\bar{\mu}\right)^{1/6}} \tag{6.2.26}$$

Equation (6.2.26) shows that decreasing the catalyst particle size and increasing the fluid velocity can significantly increase the mass-transfer coefficient. These simple variables may be used as process "handles" to decrease the influence of external mass-transfer limitations on the observed reaction rate.

To quickly estimate the importance of external mass-transfer limitations, the magnitude of the change in concentration across the boundary layer can be calculated from the observed rate and the mass-transfer coefficient:

$$r_{obs} = \bar{k}_c\left(C_{AB} - C_{AS}\right) \qquad \frac{r_{obs}}{\bar{k}_c} = \Delta C_A \tag{6.2.27}$$

If $\Delta C_A \ll C_{AB}$, then external mass-transfer limitations are not significantly affecting the observed rate.

The effects of heat transfer are completely analogous to those of mass transfer. The heat flux, q, across the stagnant boundary layer shown in Figure 6.2.1 is related to the difference in temperature and the heat-transfer coefficient, h_t, according to:

$$q = h_t\left(T_B - T_S\right) \tag{6.2.28}$$

Steady state requires that the heat flux is equivalent to the heat generated (or consumed) by reaction:

$$r_{obs}(\Delta H_r) = h_t(T_B - T_S) \tag{6.2.29}$$

where ΔH_r is the heat of reaction per mole of A converted. To estimate the influence of heat-transfer limitations on the observed rate, the change in temperature across the film is found by evaluating the observed rate of heat generated (or consumed) and the heat-transfer coefficient (obtained from J factor correlations, similar to the case of mass-transfer coefficients):

$$r_{obs}(\Delta H_r) = h_t(T_B - T_S), \qquad \frac{r_{obs}(\Delta H_r)}{h_t} = \Delta T \tag{6.2.30}$$

If $|\Delta T| \ll T_B$, then the effect of external heat-transfer limitations on the observed rate can be ignored. Equation (6.2.30) can also be used to find the maximum temperature change across the film. Using Equation (6.2.15) to eliminate the observed rate, the resulting equation relates the concentration change across the film to the temperature change:

$$\bar{k}_c(C_{AB} - C_{AS})\Delta H_r = h_t(T_B - T_S) \tag{6.2.31}$$

The maximum temperature change across the film will occur when C_{AS} approaches zero, which corresponds to the maximum observable rate. Solving Equation (6.2.31) for ΔT_{max} with $C_{AS} = 0$ gives the following expression:

$$\Delta T_{max} = \frac{\bar{k}_c \Delta H_r}{h_t} C_{AB} \tag{6.2.32}$$

that can always be calculated for a reaction, independent of an experiment. If both external heat and mass transfer are expected to affect the observed reaction rate, the balances must be solved simultaneously.

6.3 | Internal Transport Effects

Many solid catalysts contain pores in order to increase the specific surface area available for adsorption and reaction, sometimes up to 10^3 m^2 g^{-1}. Since nearly all of the catalytically active sites in highly porous solids are located in the pore network, diffusion of molecules in confined spaces obviously plays a critical role in the observed rate of reaction.

The preceding section assumed that the mass-transport mechanism in a fluid medium is dominated by molecule-molecule collisions. However, the mean free path of gases often exceeds the dimensions of small pores typical of solid catalysts. In this situation, called *Knudsen* diffusion, molecules collide more often with the pore walls than with other molecules. According to Equation (6.3.1), the Knudsen diffusivity of component A, D_{KA}, is proportional to $T^{1/2}$, but is independent of both pressure and the presence of other species:

$$D_{KA} = (9.7 \times 10^3) \cdot R_{\text{pore}} \cdot \left(\frac{T}{M_A}\right)^{1/2} \quad \text{cm}^2\,\text{s}^{-1} \tag{6.3.1}$$

where R_{pore} is the pore radius in cm, T is the absolute temperature in Kelvins, and M_A is the molecular weight of A. Recall that the diffusivity D_{AB} for molecular diffusion depends on the pressure and the other species present but is independent of the pore radius. In cases where both molecule-molecule and molecule-wall collisions are important, neither molecular diffusivity nor Knudsen diffusivity alone can adequately describe the transport phenomena. Under the conditions of equimolar counterdiffusion of a binary mixture, a transition diffusivity of component A, D_{TA}, can be approximated by the Bosanquet equation (see Appendix C for derivation):

$$\frac{1}{D_{TA}} = \frac{1}{D_{AB}} + \frac{1}{D_{KA}} \tag{6.3.2}$$

VIGNETTE 6.3.1

Diffusion of molecules in porous catalysts is highly dependent on the dimensions of the pore network. Figure 6.3.1 shows typical values of the gas-phase diffusivity as a function of pore size. Transport of molecules in very large pores is essentially governed by molecular diffusion since collisions with other molecules are much more frequent than collisions with the pore wall. In the Knudsen regime, molecule-wall collisions are dominant and the diffusivity decreases with pore size. Further reduction in pore size to values typical of zeolites results in a dramatic decrease in diffusivity due to single file diffusion of molecules. This phenomenon is also called *configurational* diffusion [P. B. Weisz,

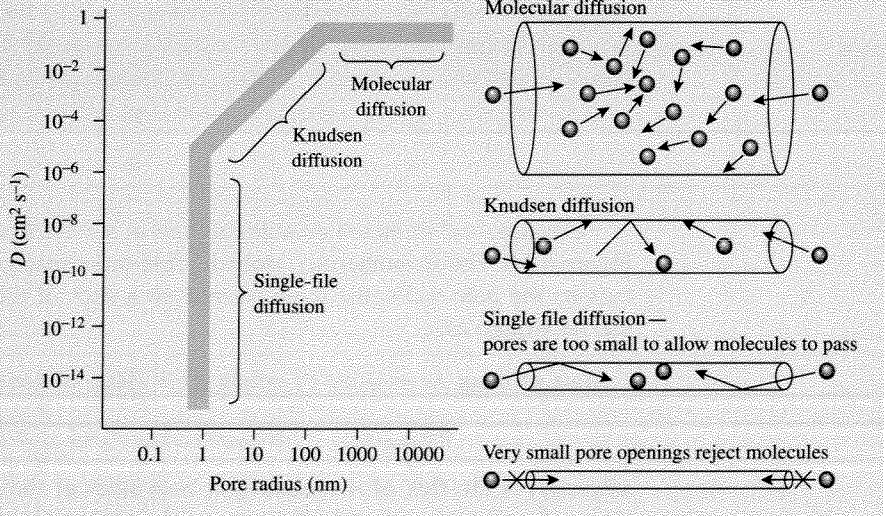

Figure 6.3.1 | Influence of pore size on diffusivity of gas-phase molecules.

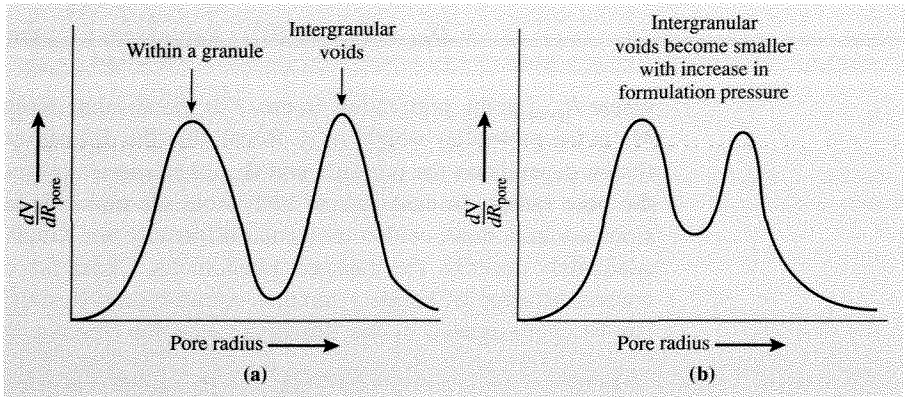

Figure 6.3.2 | Influence of pelletizing conditions on pore size distribution $\frac{dV}{dR_{pore}}$ in a bimodal pore network. **(a)** Small pores (micropores) are associated with the catalyst powder whereas large pores (macropores) result from the voids between granules in compressed catalyst pellets. **(b)** Decrease in pore size associated with intergranular voids as pellet in **(a)** is compressed as higher pressure.

CHEMTECH, (Aug. 1973) 498], and is described mathematically in a unique manner. For molecules exceeding the size of the pore aperture, the interior of the pore is inaccessible.

Small pores, called *micropores*, are often present in high surface area catalyst powders. These powders are compressed to form pellets so that the pressure drop in an industrial packed bed reactor is not too great. However, compression of the powders creates a new network of pores, called *macropores*, formed by the intergranular voids. If the original catalyst powder had a unimodal pore size distribution (PSD), the compressed catalyst pellet would have a bimodal PSD (see Figure 6.3.2.) The pore size associated with the voids is a function of the pressure used to form the pellet—high formulation pressures result in smaller void spaces. In contrast, the micropores of the catalyst powders are relatively unaffected by the compression process (see Figure 6.3.2).

Consider the idealized cylindrical pore in a solid catalyst slab, as depicted in Figure 6.3.3. For an isothermal, isobaric, first-order reaction of A to form B that occurs on the pore walls, the mole balance on a slice of the pore with thickness Δx can be written as:

$$(\text{Rate of input } A) - (\text{Rate of output } A) + (\text{Rate of generation } A) = 0 \qquad (6.3.3)$$

$$\pi R_{\text{pore}}^2 N_A\big|_x - \pi R_{\text{pore}}^2 N_A\big|_{x+\Delta x} - k_s C_A (2\pi R_{\text{pore}})(\Delta x) = 0 \qquad (6.3.4)$$

where N_A is the flux of A evaluated at both sides of the slice, k_s is the first-order rate constant expressed per surface area of the catalyst (volume/{surface area}/time), and $2\pi R_{\text{pore}}(\Delta x)$ is the area of the pore wall in the catalyst slice. Rearranging

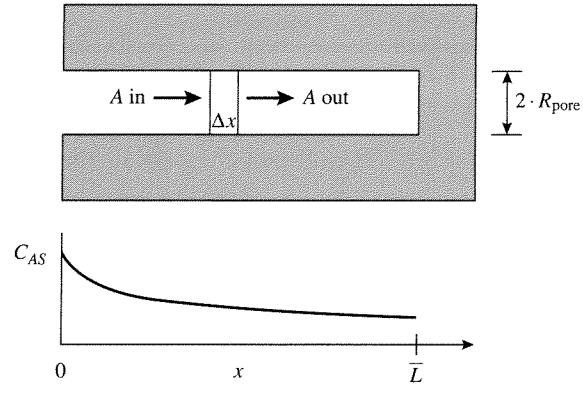

Figure 6.3.3 |
Schematic representation of component A diffusing and reacting in an idealized cylindrical pore.

Equation (6.3.4) and taking the limit as Δx approaches zero gives the following differential equation for the mole balance:

$$-\frac{dN_A}{dx} = \frac{2k_s}{R_{\text{pore}}} C_A \tag{6.3.5}$$

Recall that the Stefan-Maxwell equation relates the molar flux of A to its concentration gradient according to:

$$\nabla C_A = \sum_{\substack{j=1 \\ j \neq A}}^{n} \frac{1}{D_{Aj}} \left(X_A N_j - X_j N_A \right) \tag{6.3.6}$$

For diffusion in one dimension in the absence of bulk flow:

$$\frac{dC_A}{dx} = -\frac{N_A}{\left(\frac{1}{D_{AB}} + \frac{1}{D_{KA}} \right)^{-1}} \tag{6.3.7}$$

which is Fick's First Law that can be written as:

$$N_A = -D_{TA} \frac{dC_A}{dx} \tag{6.3.8}$$

where D_{TA} is defined by Equation (6.3.2). Substitution of Fick's Law into the mole balance, Equation (6.3.5), yields the following second-order differential equation:

$$\frac{d}{dx}\left(D_{TA} \frac{dC_A}{dx} \right) = \frac{2k_s}{R_{\text{pore}}} C_A \tag{6.3.9}$$

Assuming D_{TA} is constant:

$$\frac{d^2C_A}{dx^2} - \frac{2k_s}{D_{TA}R_{\text{pore}}}C_A = 0 \tag{6.3.10}$$

The surface rate constant can be rewritten on a volume basis by using the surface to volume ratio of a cylindrical pore:

$$\frac{\text{Area}}{\text{Volume}} = \frac{2\pi R_{\text{pore}}\bar{L}}{\pi R_{\text{pore}}^2\bar{L}} = \frac{2}{R_{\text{pore}}} \tag{6.3.11}$$

and

$$k = \frac{2k_s}{R_{\text{pore}}} \tag{6.3.12}$$

To simplify the mole balance, let:

$$\chi = \frac{x}{\bar{L}} \tag{6.3.13}$$

$$\phi = \bar{L}\sqrt{\frac{k}{D_{TA}}} \tag{6.3.14}$$

and their substitution into Equation (6.3.10) gives:

$$\frac{d^2C_A}{d\chi^2} - \phi^2 C_A = 0 \tag{6.3.15}$$

Boundary conditions at each end of the pore are needed to solve the mole balance. At $x = 0$ (the pore mouth), the concentration of A is equal to C_{AS}. At the other end of the pore, the gradient in concentration is equal to zero. That is, there is no flux at the end of the pore. These conditions can be written as:

$$C_A = C_{AS} \qquad \text{at } \chi = 0 \tag{6.3.16}$$

$$\frac{dC_A}{d\chi} = 0 \qquad \text{at } \chi = 1 \tag{6.3.17}$$

The solution of Equation (6.3.15) using boundary conditions given in Equations (6.3.16) and (6.3.17) is:

$$C_A = C_{AS}\frac{\cosh\left[\phi\left(1 - \frac{x}{\bar{L}}\right)\right]}{\cosh[\phi]} \tag{6.3.18}$$

The term ϕ, also known as the *Thiele modulus*, is a dimensionless number composed of the square root of the characteristic reaction rate (kC_{AS}) divided by the characteristic diffusion rate $\left(\frac{D_{TA}C_{AS}}{\bar{L}^2}\right)$. The Thiele modulus indicates which process

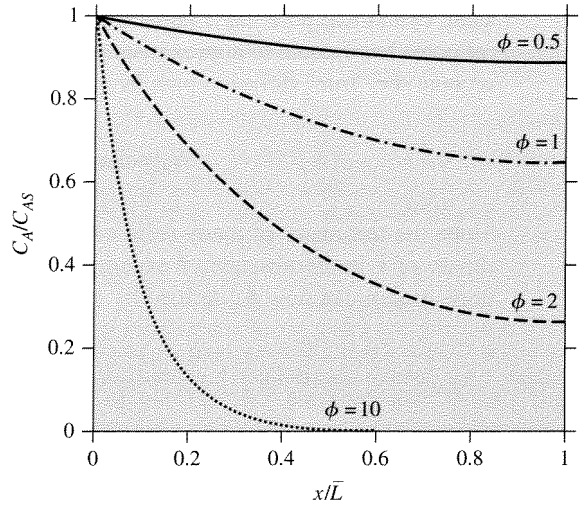

Figure 6.3.4 |
Effect of Thiele modulus on the normalized concentration profiles in a catalyst pore with first-order surface reaction.

is rate-limiting. Figure 6.3.4 illustrates the concentration profile of reactant A along the pore for various values of the Thiele modulus. When ϕ is small, the diffusional resistance is insufficient to limit the rate of reaction and the concentration can be maintained near C_{AS} within the catalyst particle. However, when ϕ is large, a significant diffusional resistance prevents a constant concentration profile of A within the catalyst particle and thus lowers the observed rate.

Now consider a catalyst pellet with a random network of "zig-zag" pores. The surface of the pellet is composed of both solid material and pores. The flux equation derived earlier must be modified to account for the fact that the flux, N_A, is based only on the area of a pore. A parameter called the *porosity* of the pellet, or $\bar{\varepsilon}_p$, is defined as the ratio of void volume within the pellet to the total pellet volume (void + solid). The flux can be expressed in moles of A diffusing per unit pellet surface area (containing both solids and pores) by using $\bar{\varepsilon}_p$ as follows:

$$N_A = \bar{\varepsilon}_p N_A(\text{based on pore}) = -\bar{\varepsilon}_p D_{TA} \frac{dC_A}{dx}$$

Since the porosity of many solid catalysts falls between 0.3 and 0.7, a reasonable estimate of $\bar{\varepsilon}_p$ in the absence of experimental data is 0.5. The second parameter needed to modify the flux is the tortuosity, $\bar{\tau}$, which accounts for the deviations in the path length of the pores. Since the concentration gradient is based on the pellet geometry, the flux equation must be corrected to reflect the actual distance molecules travel in the pores. The tortuosity is the ratio of the "zig-zag length" to the "straight length" of the pore system. Obviously, $\bar{\tau}$ must be greater than or equal to one. For example, an

ideal, cylindrical pore has $\bar{\tau}$ equal to 1, and a network of randomly oriented cylindrical pores has $\bar{\tau}$ equal to approximately 3. The flux equation can be written to take into account the "true" diffusion path length as:

$$N_A(\text{pellet}) = -\frac{\bar{\varepsilon}_p}{\bar{\tau}} D_{TA} \frac{dC_A}{dx}$$

Since the tortuosity of many solid catalysts falls between 2 and 7, a reasonable estimate of $\bar{\tau}$ in the absence of experimental data is 4. The diffusivity in a unimodal pore system can now be defined by the flux of reactant into the pellet according to:

$$N_A(\text{pellet}) = \frac{\bar{\varepsilon}_p}{\bar{\tau}} N_A(\text{pore}) = -\frac{\bar{\varepsilon}_p}{\bar{\tau}} D_{TA} \frac{dC_A}{dx} = -D_{TA}^e \frac{dC_A}{dx} \tag{6.3.19}$$

where the superscript e refers to the *effective* diffusivity. Likewise, the following *effective* diffusivities can be written:

$$D_{KA}^e = \frac{\bar{\varepsilon}_p}{\bar{\tau}} D_{KA} \tag{6.3.20}$$

$$D_{AB}^e = \frac{\bar{\varepsilon}_p}{\bar{\tau}} D_{AB} \tag{6.3.21}$$

Now consider several ideal geometries of porous catalyst pellets shown in Figure 6.3.5. The first pellet is an infinite slab with thickness $2x_p$. However, since

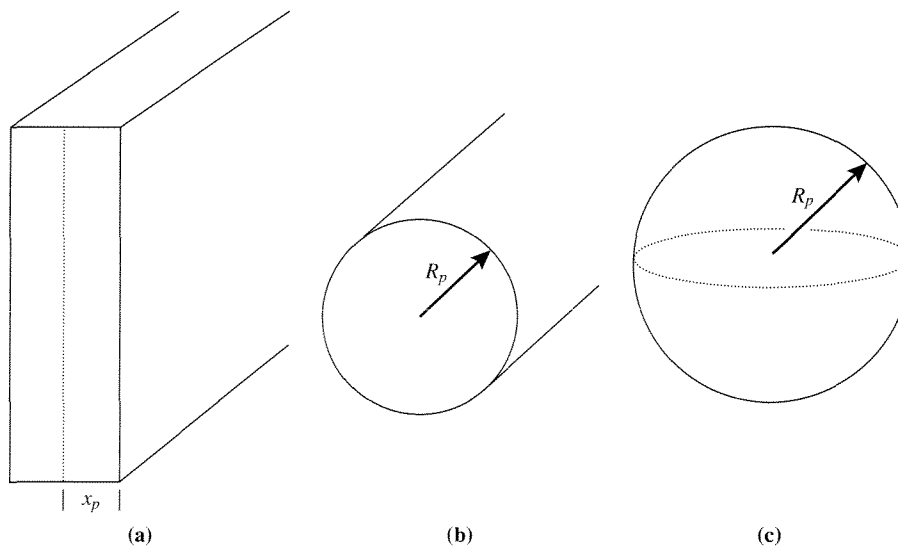

Figure 6.3.5 |
Schematic representations of ideal catalyst pellet geometries. **(a)** Infinite slab. **(b)** Infinite right cylinder. **(c)** Sphere.

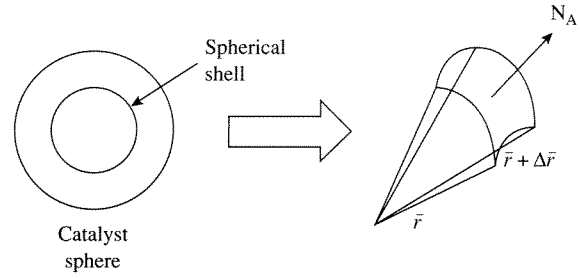

Figure 6.3.6 |
Schematic of the shell balance on a spherical catalyst pellet.

pores can have openings on both faces of the slab because of symmetry, the characteristic length associated with the slab is half of the thickness, or x_p. The second pellet is an infinite right cylinder with radius R_p, and the third pellet is a sphere with radius R_p. End effects (or edge effects) are ignored in the cases of the slab and the cylinder.

As an example, simultaneous diffusion and reaction in a spherical catalyst pellet is described in detail below. The results are then generalized to other pellet shapes. The reaction is assumed to be isothermal, since the high thermal conductivity of most solid catalysts ensures a fairly constant temperature within a single pellet. In addition, the reaction is assumed to be isobaric, which implies negligible mole change upon reaction. For reactions with a significant mole change with conversion, the presence of a large excess of inert material can reduce the impact of reacting species on the total pressure. Isobaric conditions can therefore be achieved in a variety of catalytic reactions, regardless of reaction stoichiometry.

A diagram of the shell balance (material balance) for simultaneous diffusion and first order reaction of component A in a sphere is shown in Figure 6.3.6. The material balance in the spherical shell is given by:

$$\text{(Rate of input } A) - \text{(Rate of output } A) + \text{(Rate of generation } A) = 0$$

$$4\pi\bar{r}^2 N_A|_{\bar{r}} - 4\pi\bar{r}^2 N_A|_{\bar{r}+\Delta\bar{r}} - kC_A\, 4\pi\bar{r}^2\Delta\bar{r} = 0 \qquad (6.3.22)$$

The third term in Equation (6.3.22) is the rate of consumption of A in the differential volume defined between $\bar{r}$ and $\bar{r} + \Delta\bar{r}$. Simplifying Equation (6.3.22) and taking the limit as $\Delta\bar{r}$ approaches zero yields the following differential equation:

$$-\frac{d(\bar{r}^2 N_A)}{d\bar{r}} - \bar{r}^2 k C_A = 0 \qquad (6.3.23)$$

The flux of A can be expressed in terms of concentration for binary systems according to Fick's Law (in spherical coordinates):

$$N_A = -D_{TA}^e \frac{dC_A}{d\bar{r}} \qquad \text{(equimolar counterdiffusion)} \qquad (6.3.24)$$

Substitution of Equation (6.3.24) into (6.3.23) gives:

$$-\frac{d\left[\bar{r}^2\left(-D_{TA}^e\frac{dC_A}{d\bar{r}}\right)\right]}{d\bar{r}} - \bar{r}^2kC_A = 0$$

$$D_{TA}^e\left[\bar{r}^2\frac{d^2C_A}{d\bar{r}^2} + 2\bar{r}\frac{dC_A}{d\bar{r}}\right] - \bar{r}^2kC_A = 0$$

$$D_{TA}^e\left[\frac{d^2C_A}{d\bar{r}^2} + \frac{2}{\bar{r}}\frac{dC_A}{d\bar{r}}\right] - kC_A = 0 \tag{6.3.25}$$

The above equation can be made dimensionless by the following substitutions:

$$\psi = \frac{C_A}{C_{AS}} \tag{6.3.26}$$

$$\omega = \frac{\bar{r}}{R_p} \tag{6.3.27}$$

where C_{AS} is the concentration of A on the external surface and R_p is the radius of the spherical particle. Rewriting Equation (6.3.25) in terms of dimensionless concentration and radius gives:

$$\frac{d^2\psi}{d\omega^2} + \frac{2}{\omega}\frac{d\psi}{d\omega} - \frac{(R_p)^2k}{D_{TA}^e}\psi = 0 \tag{6.3.28}$$

The Thiele modulus, ϕ, for a sphere is defined as:

$$\phi = R_p\sqrt{\frac{k}{D_{TA}^e}} \tag{6.3.29}$$

so that Equation (6.3.28) becomes:

$$\frac{d^2\psi}{d\omega^2} + \frac{2}{\omega}\frac{d\psi}{d\omega} - \phi^2\psi = 0 \tag{6.3.30}$$

with boundary conditions:

$$\psi = 1 \qquad \text{at } \omega = 1 \quad \text{(surface of sphere)} \tag{6.3.31}$$

$$\frac{d\psi}{d\omega} = 0 \qquad \text{at } \omega = 0 \quad \text{(center of sphere)} \tag{6.3.32}$$

The zero-flux condition at the center results from the symmetry associated with the spherical geometry. The solution of the above differential equation with the stated boundary conditions is:

$$\psi = \frac{C_A}{C_{AS}} = \frac{\sinh(\phi\omega)}{\omega\sinh(\phi)} \tag{6.3.33}$$

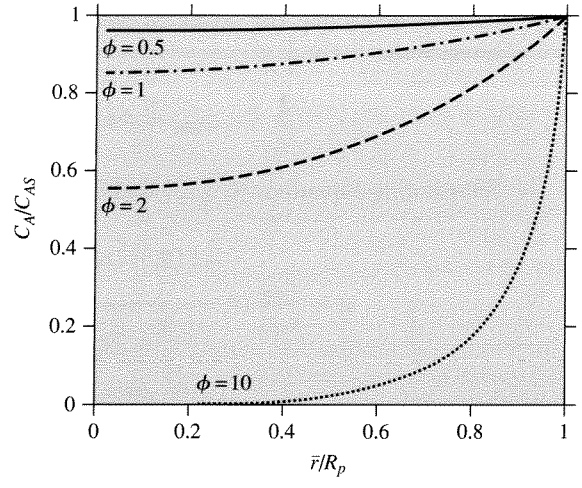

Figure 6.3.7 |
Effect of Thiele modulus on the normalized concentration profiles in a spherical catalyst particle with first-order reaction. The external surface of the particle is located at $\bar{r}/R_p = 1$.

Figure 6.3.7 illustrates the effect of the Thiele modulus on the concentration profile within a spherical catalyst pellet.

An *effectiveness factor,* η, can be defined as the ratio of the observed rate (r_{obs}) to the rate that would be observed in the absence of internal diffusional limitations (r_{max}):

$$\eta = \frac{r_{obs}}{r_{max}} = \frac{\int_0^{V_p} r(C_A)\,dV}{V_p r(C_{AS})} = \frac{\int_0^{R_p} r(C_A) 4\pi \bar{r}^2 d\bar{r}}{V_p r(C_{AS})} = \frac{S_p \int_0^{R_p} r(C_A)\left(\frac{\bar{r}}{R_p}\right)^2 d\bar{r}}{V_p r(C_{AS})} \quad (6.3.34)$$

where V_p is the volume of the catalyst pellet, S_p is the external surface area of the pellet, and $r(C_A)$ is the reaction rate determined with concentration C_A. The denominator in Equation (6.3.34) is simply the rate of reaction in the catalyst pellet assuming the reactant concentration is equal to that on the external surface, C_{AS}. For a first-order reaction in a spherical particle, the rate observed in the absence of diffusional limitations is:

$$r_{max} = \frac{4}{3}\pi (R_p)^3 k C_{AS} \quad (6.3.35)$$

At the steady state, the flux of A entering the pellet must be equivalent to the net rate of consumption of A in the pellet. Thus, the flux entering the sphere can be

used to determine the observed rate of reaction in the presence of diffusional limitations.

$$r_{obs} = 4\pi (R_p)^2 D_{TA}^e \frac{dC_A}{d\bar{r}}\bigg|_{\bar{r}=R_p} \tag{6.3.36}$$

Substituting Equations (6.3.35) and (6.3.36) into (6.3.34) gives:

$$\eta = \frac{r_{obs}}{r_{max}} = \frac{4\pi (R_p)^2 D_{TA}^e \left.\dfrac{dC_A}{d\bar{r}}\right|_{\bar{r}=R_p}}{\dfrac{4}{3}\pi (R_p)^3 k C_{AS}} = \frac{3}{R_p}\frac{D_{TA}^e}{k}\frac{\left.\dfrac{dC_A}{d\bar{r}}\right|_{\bar{r}=R_p}}{C_{AS}} \tag{6.3.37}$$

The above equation is made nondimensional by the substitutions defined in Equations (6.3.26) and (6.3.27) and is:

$$\eta = \frac{3}{\phi^2}\frac{d\psi}{d\omega}\bigg|_{\omega=1} \tag{6.3.38}$$

The derivative is evaluated from the concentration profile, (6.3.33), to give:

$$\eta = \frac{3}{\phi^2}\frac{d\psi}{d\omega}\bigg|_{\omega=1} = \frac{3}{\phi^2}\frac{d}{d\omega}\left[\frac{\sinh(\phi\omega)}{\omega\sinh(\phi)}\right]\bigg|_{\omega=1}$$

$$\eta = \frac{3}{\phi^2}\left[\frac{1}{\sinh(\phi)}\left(\frac{\phi}{\omega}\cosh(\phi\omega) - \frac{1}{\omega^2}\sinh(\phi\omega)\right)\right]\bigg|_{\omega=1}$$

$$\eta = \frac{3}{\phi^2}\left[\frac{\phi}{\tanh(\phi)} - 1\right] = \frac{3}{\phi}\left[\frac{1}{\tanh(\phi)} - \frac{1}{\phi}\right] \tag{6.3.39}$$

Figure 6.3.8 illustrates the relationship between the effectiveness factor and the Thiele modulus for a spherical catalyst pellet.

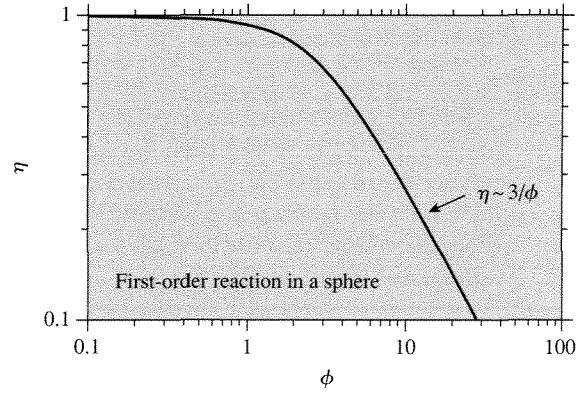

Figure 6.3.8 |
Effectiveness factor for a first-order reaction in a sphere as a function of the Thiele modulus.

Table 6.3.1 | Influence of catalyst particle geometry on concentration profile and effectiveness factor for a first-order, isothermal, isobaric reaction.

	Slab ($\omega = x/x_p$)	Cylinder[(a)] ($\omega = \bar{r}/R_p$)	Sphere ($\omega = \bar{r}/R_p$)
ϕ	$x_p\sqrt{\dfrac{k}{D_{TA}^e}}$	$R_p\sqrt{\dfrac{k}{D_{TA}^e}}$	$R_p\sqrt{\dfrac{k}{D_{TA}^e}}$
$\psi = C_A/C_{AS}$	$\dfrac{\cosh(\phi\omega)}{\cosh(\phi)}$	$\dfrac{I_0(\phi\omega)}{I_0(\phi)}$	$\dfrac{\sinh(\phi\omega)}{\omega\sinh(\phi)}$
η	$\dfrac{\tanh(\phi)}{\phi}$	$\dfrac{2I_1(\phi)}{\phi I_0(\phi)}$	$\dfrac{3}{\phi}\left[\dfrac{1}{\tanh(\phi)} - \dfrac{1}{\phi}\right]$

[(a)] I_i is a modified Bessel function of order i.

Table 6.3.2 | Characteristic length parameters of common pellet shapes.

	L_p
Slab	Length of pore, x_p
Cylinder	$R_p/2$
Sphere	$R_p/3$

A low value of the Thiele modulus results from a small diffusional resistance. For this case, the effectiveness factor is approximately 1 (values of ϕ typically less than 1). Large values of the Thiele modulus are characteristic of a diffusion-limited reaction with an effectiveness factor less than 1. For $\phi \gg 1$, the value of the effectiveness factor in a sphere approaches $3/\phi$, as illustrated in Figure 6.3.8.

The concentration profile and the effectiveness factor are clearly dependent on the geometry of a catalyst particle. Table 6.3.1 summarizes the results for catalyst particles with three common geometries.

Aris was the first to point out that the results for the effectiveness factor in different pellet geometries can be approximated by a single function of the Thiele modulus if the length parameter in ϕ is the ratio of the pellet volume, V_p, to the pellet external surface area, S_p [R. Aris, *Chem. Eng. Sci.*, **6** (1957) 262]. Thus, the length parameter, L_p, is defined by:

$$L_p = \frac{V_p}{S_p} \tag{6.3.40}$$

and the Thiele modulus is defined by:

$$\phi_0 = L_p\sqrt{\frac{k}{D_{TA}^e}} \tag{6.3.41}$$

where Table 6.3.2 summarizes the characteristic length parameter for common geometries.

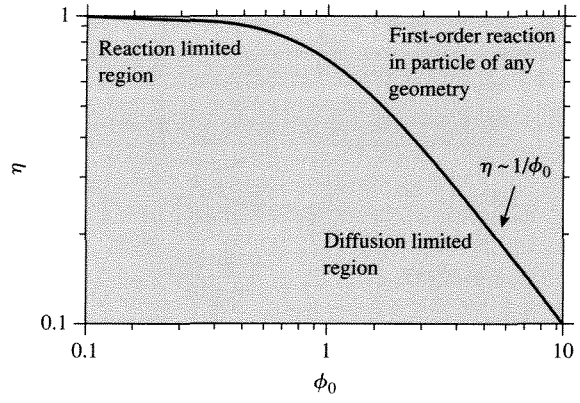

Figure 6.3.9 |
Effectiveness factor $[\eta = \tanh(\phi_0)/\phi_0]$ for a first-order reaction in a catalyst as a function of the Thiele modulus with generalized length parameter.

According to the above definitions, the effectiveness factor for any of the above shapes can adequately describe simultaneous reaction and diffusion in a catalyst particle. The equation for the effectiveness factor in a slab is the simplest in Table 6.3.1 and will be used for all pellet shapes with the appropriate Thiele modulus:

$$\eta = \frac{\tanh(\phi_0)}{\phi_0} \tag{6.3.42}$$

This relationship is plotted in Figure 6.3.9. The effectiveness factor for a severely diffusion-limited reaction in a catalyst particle is approximated by the inverse of the Thiele modulus.

EXAMPLE 6.3.1 |

The double bond isomerization of 1-hexene to form 2-hexene was studied in a laboratory reactor containing rhodium particles supported on alumina at 150°C and atmospheric pressure:

$$H_2C{=}CH{-}CH_2{-}CH_2{-}CH_2{-}CH_3 \Rightarrow H_3C{-}CH{=}CH{-}CH_2{-}CH_2{-}CH_3$$

The reaction was found to be first order in 1-hexene with a rate constant of 0.14 s^{-1}. Find the largest pellet size that can be used in an industrial reactor to achieve 70 percent of the maximum rate. The pore radius of the alumina is 10 nm, and D_{AB} is 0.050 $cm^2\ s^{-1}$.

■ Answer

It is desired to find the particle size that gives an internal effectiveness factor equal to 0.70. For any geometry, the Thiele modulus is determined from:

$$\eta = \frac{\tanh(\phi_0)}{\phi_0} = 0.70$$

$$\phi_0 = 1.18$$

Assuming a spherical catalyst pellet with radius R_p, the Thiele modulus is:

$$\phi_0 = 1.18 = \frac{V_p}{S_p}\sqrt{\frac{k}{D^e_{TA}}} = \frac{R_p}{3}\sqrt{\frac{k}{D^e_{TA}}}$$

Since the rate constant is known, estimation of the effective diffusivity allows the calculation of particle radius. In the absence of experimental data, the porosity and tortuosity are assumed to be 0.5 and 4, respectively. Thus,

$$D^e_{AB} = \frac{\bar{\varepsilon}_p}{\bar{\tau}} D_{AB} = \frac{0.5}{4} \cdot 0.050 = 0.0062 \text{ cm}^2 \text{ s}^{-1}$$

The Knudsen diffusivity is calculated from the temperature, pore radius, and molecular weight of hexene (84 g mol^{-1}) according to Equation (6.3.1):

$$D_{KA} = (9.7 \times 10^3) \cdot R_{\text{pore}} \cdot \sqrt{\frac{T}{M_A}} \quad (\text{cm}^2 \text{ s}^{-1})$$

$$D_{KA} = (9.7 \times 10^3)(1.0 \times 10^{-6}\text{cm})\sqrt{\frac{423K}{84}} = 0.022 \text{ cm}^2 \text{ s}^{-1}$$

$$D^e_{KA} = \frac{0.5}{4} \cdot 0.022 = 0.0027 \text{ cm}^2 \text{ s}^{-1}$$

The effective transition diffusivity is calculated from the Bosanquet equation assuming equimolar counter diffusion, which is what happens with isomerization reactions:

$$\frac{1}{D^e_{TA}} = \frac{1}{D^e_{AB}} + \frac{1}{D^e_{KA}}$$

$$D^e_{TA} = 0.0019 \text{ cm}^2 \text{ s}^{-1}$$

Substituting the necessary terms into the expression for the Thiele modulus yields the radius of the spherical catalyst pellet:

$$R_p = 3 \cdot 1.18 \cdot \sqrt{\frac{0.0019}{0.14}} = 0.41 \text{ cm}$$

Thus, spherical particles of about 1/3 in. diameter will have an effectiveness factor of 0.70.

It is worthwhile to examine how reasonably well a single characteristic length parameter describes reaction/diffusion in a finite cylinder, a very common catalyst pellet configuration. The pellet shown has a cylinder length ($2x_p$) and radius R_p:

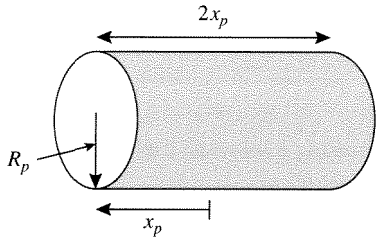

The material balance for a first-order reaction of A in the pellet is given by:

$$D_{TA}^{e}\left[\frac{\partial^2 C_A}{\partial \bar{r}^2}+\frac{1}{\bar{r}}\frac{\partial C_A}{\partial \bar{r}}+\frac{\partial^2 C_A}{\partial x^2}\right]=kC_A \tag{6.3.43}$$

with the flux equations being written for both the axial and radial directions:

$$N_A=-D_{TA}^{e}\frac{dC_A}{d\bar{r}} \quad \text{(radial)} \tag{6.3.44}$$

$$N_A=-D_{TA}^{e}\frac{dC_A}{dx} \quad \text{(axial)} \tag{6.3.45}$$

The solution of these equations, with appropriate boundary conditions, provides the concentration profile and the effectiveness factor for a finite cylinder. As discussed earlier, an approximation of the effectiveness factor:

$$\eta=\frac{\tanh(\phi_0)}{\phi_0} \tag{6.3.42}$$

can be used with any geometry as long as the Thiele modulus is based on the characteristic length defined by the volume-to-surface ratio. The volume and surface area of the finite cylindrical pellet are simply:

$$V_p=\pi(R_p)^2\cdot 2x_p \tag{6.3.46}$$

$$S_p=2\pi\,(R_p)^2+\left(2\pi R_p\cdot 2x_p\right) \tag{6.3.47}$$

Thus, the characteristic length for the finite cylinder is:

$$\frac{V_p}{S_p}=\frac{\pi(R_p)^2\cdot 2x_p}{2\pi(R_p)^2+\left(2\pi R_p\cdot 2x_p\right)}=\frac{R_p}{\dfrac{R_p}{x_p}+2} \tag{6.3.48}$$

and the Thiele modulus for use in Equation (6.3.42) is:

$$\phi_0=\frac{V_p}{S_p}\sqrt{\frac{k}{D_{TA}^{e}}}=\left[\frac{R_p}{\dfrac{R_p}{x_p}+2}\right]\sqrt{\frac{k}{D_{TA}^{e}}} \tag{6.3.49}$$

For comparison, the "radius" of an "equivalent" spherical particle, $R_{p(\text{sphere})}$, can be calculated by equating the volume-to-surface ratios:

$$\left(\frac{V_p}{S_p}\right)_{\text{finite cylinder}} = \left(\frac{V_p}{S_p}\right)_{\text{sphere}}$$

$$\frac{R_p}{\frac{R_p}{x_p} + 2} = \frac{R_{p(\text{sphere})}}{3}$$

Therefore, the radius of an "equivalent" sphere is:

$$R_{p(\text{sphere})} = 3\left(\frac{R_p}{\frac{R_p}{x_p} + 2}\right) \tag{6.3.50}$$

which can be used to evaluate the Thiele modulus and effectiveness factor. Figure 6.3.10 compares the effectiveness factor derived from the full solution of the material balance for a finite cylinder (individual points) to the approximate solution using the "equivalent" radius of a sphere based on the volume to surface ratio. Also shown is the solution for an infinite cylinder with equal (V_p/S_p). Clearly, the agreement among the sets of results confirms that substituting the characteristic

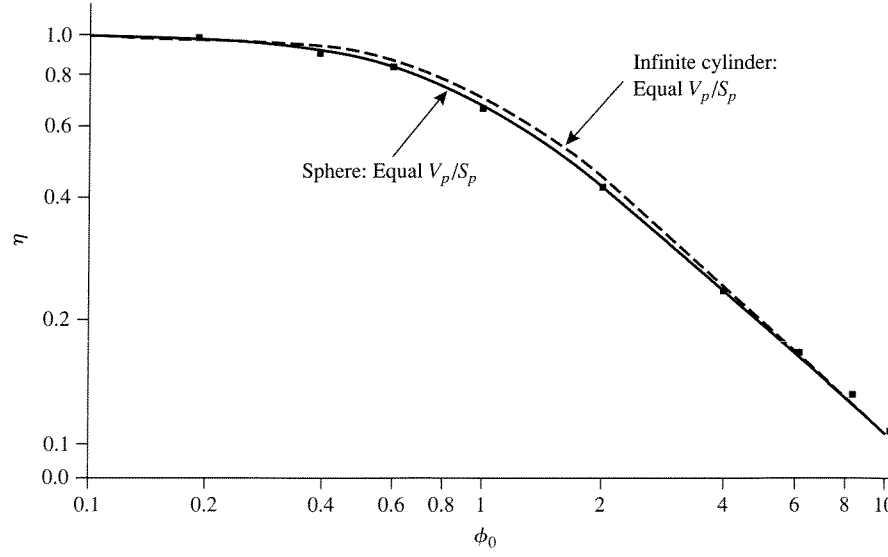

Figure 6.3.10 |
Effectiveness factors for sphere, infinite cylinder, and finite cylinder pellet geometries where the Thiele modulus is based on equal V_p/S_p. Individual points correspond to the numerical solutions of the material balance on a finite cylinder.

length in the Thiele modulus by (V_p/S_p) is an excellent approximation to the true solution.

EXAMPLE 6.3.2

The rate constant for the first-order cracking of cumene on a silica-alumina catalyst was measured to be 0.80 $cm^3/(s \cdot gcat)$ in a laboratory reactor:

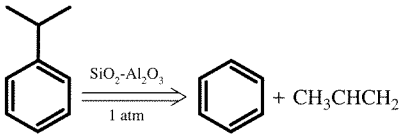

Is the observed rate constant the true rate constant or is there influence of pore diffusion? Additional data:

$$R_p = 0.25 \text{ cm}$$
$$\rho = 1.2 \text{ gcat cm}^{-3}$$
$$D_{TA}^e = 1.0 \times 10^{-3} \text{ cm}^2 \text{ s}^{-1}$$

■ Answer

Recall that the effectiveness factor can be approximated by:

$$\eta = \frac{\tanh(\phi_0)}{\phi_0}$$

when the Thiele modulus is defined in terms of the characteristic length of a pellet:

$$\phi_0 = L_p \sqrt{\frac{k}{D_{TA}^e}}$$

For the spherical particles in this problem:

$$\phi_0 = L_p \sqrt{\frac{k}{D_{TA}^e}} = \frac{R_p}{3} \sqrt{\frac{k}{D_{TA}^e}} = \left(\frac{(0.25)(\text{cm})}{3}\right) \sqrt{\frac{k\left(\frac{\text{cm}^3}{\text{s} \cdot \text{gcat}}\right) \cdot 1.2\left(\frac{\text{gcat}}{\text{cm}^3}\right)}{1.0 \times 10^{-3}\left(\frac{\text{cm}^2}{\text{s}}\right)}} = 2.9\sqrt{k}$$

Since the observed rate is first-order:

$$r_{obs} = k_{obs} C_{AS}$$

and, by definition, the effectiveness factor is:

$$\eta = \frac{\text{observed rate}}{\text{rate in absence of diffusion}} = \frac{k_{obs} C_{AS}}{k C_{AS}}$$

Substitute the Thiele modulus into the expression for the effectiveness factor to solve for k, the true rate constant, by trial and error:

$$\eta = \frac{\tanh(\phi_0)}{\phi_0} = \frac{\tanh(2.9\sqrt{k})}{2.9\sqrt{k}} = \frac{k_{\text{obs}}}{k} = \frac{0.80}{k}$$

$$k = 5.4 \frac{\text{cm}^3}{\text{s} \cdot \text{gcat}} \quad \eta = 0.15$$

Since η is small, there is a great influence of pore diffusion on the observed rate.

The material balance for simultaneous reaction and diffusion in a catalyst pellet can be extended to include more complex reactions. For example, the generalized Thiele modulus for an irreversible reaction of order n is:

$$\phi_0 = \frac{V_p}{S_p}\sqrt{\frac{n+1}{2}\frac{kC_{AS}^{n-1}}{D_{TA}^e}} \qquad n > -1 \tag{6.3.51}$$

The generalized modulus defined in Equation (6.3.51) has been normalized so that the effectiveness factor is approximately $1/\phi_0$ at large values of ϕ_0, as illustrated in Figure 6.3.9.

The implications of severe diffusional resistance on observed reaction kinetics can be determined by simple analysis of this more general Thiele modulus. The observed rate of reaction can be written in terms of the intrinsic rate expression and the effectiveness factor as:

$$r_{\text{obs}} = \eta k C_{AS}^n \tag{6.3.52}$$

As discussed earlier, the effectiveness factor is simply the inverse of the Thiele modulus for the case of severe diffusional limitations (Figure 6.3.9.) Thus, the observed rate under strong diffusional limitations can be written as:

$$r_{\text{obs}} = \frac{1}{\phi_0} k C_{AS}^n \tag{6.3.53}$$

Substitution of the generalized Thiele modulus, Equation (6.3.51), into (6.3.53) gives the following expression for the observed rate:

$$r_{\text{obs}} = \frac{S_p}{V_p}\left(\frac{2}{n+1} D_{TA}^e k\right)^{\frac{1}{2}} C_{AS}^{(n+1)/2} = k_{\text{obs}} C_A^{n_{\text{obs}}} \tag{6.3.54}$$

The order of reaction observed under conditions of severe diffusional limitations, n_{obs}, becomes $(n+1)/2$ instead of the true reaction order n. The temperature dependence of the rate is also affected by diffusional limitations. Since the observed rate constant, k_{obs}, is proportional to $(D_{TA}^e k)^{\frac{1}{2}}$, the observed activation energy is $(E_D + E)/2$, where E_D is the activation energy for diffusion and E is the activation energy for reaction. Diffusional processes are weakly activated compared to chemical

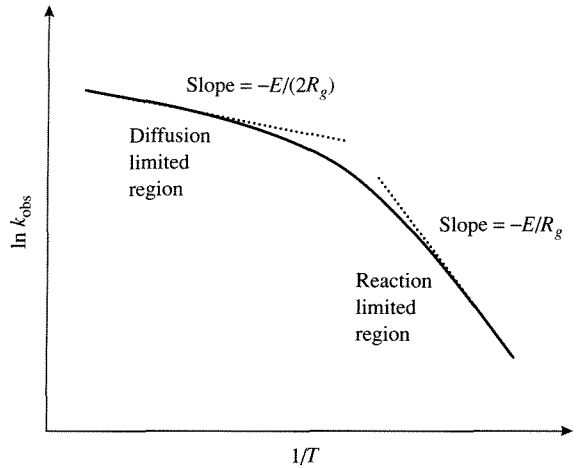

Figure 6.3.11 |
Temperature dependence of the observed rate constant of a reaction occurring in a porous catalyst pellet.

reactions, and the value of E_D can often be neglected compared to E. Thus, the observed activation energy for a severely diffusion-limited reaction is approximately one half the true value. An Arrhenius plot of the *observed* rate constant, shown in Figure 6.3.11, illustrates the effect of diffusional resistances on the *observed* activation energy. At low temperatures, the reaction rate is not limited by diffusional resistances, and the observed activation energy is the true value. At high temperatures, the reaction rate is inhibited by diffusional resistances, and the activation energy is half the true value.

EXAMPLE 6.3.3

Develop expressions for the Thiele modulus and the concentration profile of A for the following *reversible* first-order reaction that takes place in a flat plate catalyst pellet:

$$A = B, \quad K = \frac{k_1}{k_{-1}}$$

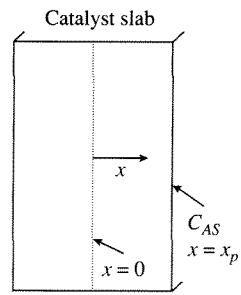

■ Answer

The material balance for diffusion/reaction in one dimension is given by:

$$\frac{d\left[-D_{TA}^{e}\frac{dC_A}{dx}\right]}{dx} = -\mathrm{r} = -[k_1C_A - k_{-1}C_B] \tag{6.3.55}$$

With C representing the total concentration, $C_A + C_B$, the rate expression can be rewritten in terms of C and C_A, thus eliminating the explicit dependence on C_B:

$$\mathrm{r} = k_1C_A - k_{-1}(C - C_A) = k_1\left(1 + \frac{1}{K}\right)C_A - \frac{k_1}{K}C = k_1\left(\frac{K+1}{K}\right)\left(C_A - \frac{C}{K+1}\right)$$

Assuming D_{TA}^{e} is constant, the following equation can be solved for the concentration profile:

$$D_{TA}^{e}\frac{d^2C_A}{dx^2} = k_1\left(\frac{K+1}{K}\right)\left(C_A - \frac{C}{K+1}\right) \tag{6.3.56}$$

with boundary conditions:

$$C_A = C_{AS} \qquad \text{at } x = x_p \quad \text{(external surface of the slab)} \tag{6.3.57}$$

$$\frac{dC_A}{dx} = 0 \qquad \text{at } x = 0 \quad \text{(center line, point of symmetry)} \tag{6.3.58}$$

The following change of variables facilitates solution of the problem. Let $\overline{\psi} = C_A - C/(K+1)$ and $\chi = x/x_p$ so that the material balance can be written as:

$$\frac{d^2\overline{\psi}}{d\chi^2} = (x_p)^2\frac{k_1}{D_{TA}^{e}}\left(\frac{1+K}{K}\right)\overline{\psi} = \phi^2\overline{\psi} \tag{6.3.59}$$

By expressing the material balance in this form, the Thiele modulus appears as the dimensionless constant ϕ:

$$\phi = x_p\sqrt{\frac{k_1}{D_{TA}^{e}}\left(\frac{1+K}{K}\right)} \tag{6.3.60}$$

The general solution of Equation (6.3.59), with arbitrary constants $\overline{\alpha}_1$ and $\overline{\alpha}_2$, is:

$$\overline{\psi} = \overline{\alpha}_1\sinh(\phi\chi) + \overline{\alpha}_2\cosh(\phi\chi) \tag{6.3.61}$$

The boundary conditions expressed in terms of the variables that are used to evaluate the constants $\overline{\alpha}_1$ and $\overline{\alpha}_2$ are:

$$\overline{\psi} = C_{AS} - \frac{C}{K+1} \qquad \text{at } \chi = 1 \tag{6.3.62}$$

$$\frac{d\overline{\psi}}{d\chi} = 0 \qquad \text{at } \chi = 0 \tag{6.3.63}$$

The constant $\bar{\alpha}_1$ vanishes due to the second boundary condition [Equation (6.3.63)]:

$$\frac{d\bar{\psi}}{d\chi} = \bar{\alpha}_1\phi\cosh(0) + \bar{\alpha}_2\phi\sinh(0) = 0$$

and

$$\cosh(0) = 1$$

so

$$\bar{\alpha}_1 = 0$$

The first boundary condition is used to evaluate $\bar{\alpha}_2$ and thus completes the solution of the problem as shown below:

$$C_{AS} - \frac{C}{K+1} = \bar{\alpha}_2\cosh(\phi)$$

$$\bar{\alpha}_2 = \frac{C_{AS} - \dfrac{C}{K+1}}{\cosh(\phi)}$$

$$\bar{\psi} = \left(C_{AS} - \frac{C}{K+1}\right)\frac{\cosh(\phi\chi)}{\cosh(\phi)} \tag{6.3.64}$$

$$C_A - \frac{C}{K+1} = \left(C_{AS} - \frac{C}{K+1}\right)\frac{\cosh\left(\phi\dfrac{x}{x_p}\right)}{\cosh(\phi)}$$

$$C_A = \frac{C}{K+1} + \left(C_{AS} - \frac{C}{K+1}\right)\frac{\cosh\left(\phi\dfrac{x}{x_p}\right)}{\cosh(\phi)} \tag{6.3.65}$$

where the Thiele modulus is defined by:

$$\phi = x_p\sqrt{\frac{k_1}{D_{TA}^e}\left(\frac{1+K}{K}\right)} \tag{6.3.60}$$

EXAMPLE 6.3.4

Set up the equations necessary to calculate the effectiveness factor for a flat-plate catalyst pellet in which the following isothermal reaction takes place:

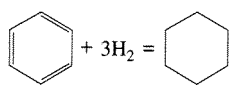

Benzene Cyclohexane

■ Answer

To solve this problem, the Stefan-Maxwell relations for molecular diffusion in a multicomponent gas mixture (see Appendix C for details) should be used:

$$\nabla X_i = \sum_{\substack{j=1 \\ j \neq i}}^{n} \frac{1}{C D_{ij}} (X_i N_j - X_j N_i)$$

For the case of diffusion in one dimension within a porous medium, these equations yield the following expression, which is derived in Appendix C:

$$-\frac{1}{R_g T}\frac{dP_i}{dx} = \sum_{j \neq i}\left(\frac{X_j N_i - X_i N_j}{D_{ij}^e}\right) + \frac{N_i}{D_{Ki}^e} \tag{6.3.66}$$

The above equation reduces to a familiar form for two components if equimolar counterdiffusion of A and B ($N_A = -N_B$) at constant temperature is assumed:

$$-\frac{1}{R_g T}\frac{dP_A}{dx} = \frac{X_B N_A - X_A N_B}{D_{AB}^e} + \frac{N_A}{D_{KA}^e} = N_A\left(\frac{1}{D_{AB}^e} + \frac{1}{D_{KA}^e}\right)$$

$$N_A = -\left(\frac{1}{\dfrac{1}{D_{AB}^e} + \dfrac{1}{D_{KA}^e}}\right)\frac{d\left(\dfrac{P_A}{R_g T}\right)}{dx} = -D_{TA}^e \frac{dC_A}{dx} \tag{6.3.67}$$

Recall this equation is similar to Equation (6.3.7) for the flux of A in one dimension. To solve the multicomponent diffusion/reaction problem of benzene hydrogenation in one dimension, Equation (6.3.66) must instead be used. First, let:

Benzene = component 1

Dihydrogen = component 2

Cyclohexane = component 3

The following diffusivities (Knudsen and binary) need to be determined from tabulated data, handbooks, correlations, theoretical equations, etc.:

Benzene: D_{K1}, D_{12}, D_{13}

Dihydrogen: D_{K2}, D_{21}, D_{23}

Cyclohexane: D_{K3}, D_{31}, D_{32}

The porosity ($\bar{\varepsilon}_p$) and tortuosity ($\bar{\tau}$) of the flat plate catalyst pellet are then used to calculate the *effective* diffusivities associated with each component according to:

$$D_{Ki}^e = \frac{\bar{\varepsilon}_p}{\bar{\tau}} D_{Ki} \tag{6.3.68}$$

$$D_{ij}^e = \frac{\bar{\varepsilon}_p}{\bar{\tau}} D_{ij} \tag{6.3.69}$$

From the stoichiometry of the hydrogenation reaction, the ratios of the fluxes of the components are:

$$\frac{N_2}{N_1} = 3 \quad \text{and} \quad \frac{N_3}{N_1} = -1$$

Substitution of these relations into Equation (6.3.66) gives the appropriate flux equations:

$$-\frac{P}{R_g T}\frac{dX_1}{dx} = N_1\left[\left(\frac{X_2 - 3X_1}{D^e_{12}} + \frac{X_3 + X_1}{D^e_{13}}\right) + \frac{1}{D^e_{K1}}\right] \tag{6.3.70}$$

$$-\frac{P}{R_g T}\frac{dX_2}{dx} = N_1\left[\left(\frac{3X_1 - X_2}{D^e_{21}} + \frac{3X_3 + X_2}{D^e_{23}}\right) + \frac{3}{D^e_{K2}}\right] \tag{6.3.71}$$

Finally, the material balance on a slice of the catalyst pellet that is needed to completely specify the reaction/diffusion problem is:

$$-\frac{dN_1}{dx} = \text{Rate}(X_1, X_2) \tag{6.3.72}$$

Rate (X_1, X_2) is the rate expression for benzene hydrogenation that depends on X_1 and X_2. For example, the following rate equation could be used if the constants $\bar{\alpha}_A$ and $\bar{\alpha}_B$ were known at the reaction temperature:

$$\text{Rate}(X_1, X_2) = \frac{\bar{\alpha}_A X_1 X_2 P^2}{1 + \bar{\alpha}_B X_1 P} \tag{6.3.73}$$

The three equations representing the material balance and the flux relations can be solved simultaneously to determine the dependent variables (X_1, X_2, and N_1) as a function of the independent variable x. (Recall that X_3 can be expressed in terms of X_1 and X_2: $1 = X_1 + X_2 + X_3$.) The boundary conditions for these equations are:

$$X_1 = X_{1S} \quad \text{and} \quad X_2 = X_{2S} \qquad \text{at } x = x_s \quad \text{(external surface of pellet)}$$

$$N_1 = 0 \qquad \text{at } x = 0 \quad \text{(center line of the slab)}$$

To calculate the effectiveness factor, the actual reaction rate throughout the catalyst is divided by the rate determined at the conditions of the external surface, that is, Rate(X_{1S}, X_{2S}). The overall reaction rate throughout the particle is equivalent to the flux N_1 evaluated at the external surface of the catalyst. Thus, the final solution is:

$$\eta = \frac{N_1|_{x=x_S}}{\text{Rate}(X_{1S}, X_{2S})} \cdot \left(\frac{S_p}{V_p}\right) \tag{6.3.74}$$

The temperature profile in the catalyst pellet can be easily incorporated into this solution by including the energy balance in the system of equations.

The previous discussion focused on simultaneous diffusion and reaction in isothermal catalyst pellets. Since ΔH_r is significant for many industrially relevant reactions, it is necessary to address how heat transfer might affect solid-catalyzed

reactions. For isothermal catalyst pellets, the effectiveness factor is less than or equal to unity, as illustrated in Figure 6.3.9. This is rationalized by examining the terms that comprise the effectiveness factor for the reaction of A in a flat plate catalyst pellet:

$$\eta = \frac{\mathrm{r}_{\mathrm{obs}}}{\mathrm{r}_{\max}} = \frac{S_p \int_0^{x_p} \mathrm{r}(C_A)\, dx}{V_p \mathrm{r}(C_{AS})} \tag{6.3.75}$$

For an isothermal pellet:

$$\int_0^{x_p} \mathrm{r}(C_A) dx \leq \mathrm{r}(C_{AS}) \tag{6.3.76}$$

If, as stated in Chapter 1, the rate is separable into two parts, one dependent on the temperature and the other dependent on the concentrations of reacting species, that is,

$$\mathrm{r} = k(T) \cdot \overline{F}(C_A) \tag{6.3.77}$$

then the concentration of A inside the pellet is less than that on the external surface,

$$\overline{F}(C_A) \leq \overline{F}(C_{AS}) \tag{6.3.78}$$

for reactions with nonnegative reaction orders. Thus,

$$\int_0^{x_p} \overline{F}(C_A) dx \leq \overline{F}(C_{AS}) \tag{6.3.79}$$

and explains the upper limit of unity for the isothermal effectiveness factor in a catalyst pellet. The situation can be very different for a nonisothermal pellet. For example, the temperature dependence of the reaction rate constant, $k(T)$, is generally expressed in an Arrhenius form

$$k(T) = \overline{A} \exp\left(\frac{-E}{R_g T}\right) \tag{6.3.80}$$

For an endothermic reaction in the presence of significant heat-transfer resistance, the temperature at the surface of the pellet can exceed the temperature of the interior, which according to Equation (6.3.80), gives:

$$k(T) \leq k(T_S) \tag{6.3.81}$$

Since $\overline{F}(C_A) \leq \overline{F}(C_{AS})$ as discussed above, the effectiveness factor is always less than or equal to unity for an endothermic reaction. For an exothermic reaction, the opposite situation can occur. The temperature of the interior of the particle can exceed the surface temperature, $T > T_S$, which leads to:

$$k(T) \geq k(T_S) \tag{6.3.82}$$

Recall that $k(T)$ is a strong function of temperature. The effectiveness factor for an exothermic reaction can be less than, equal to, or greater than unity, depending on how $k(T)$ increases relative to $\overline{F}(C_A)$ within the particle. Thus, there are cases where the increase in $k(T)$ can be much larger than the decrease in $\overline{F}(C_A)$, for example,

$$k(T) \cdot \overline{F}(C_A) > k(T_S) \cdot \overline{F}(C_{AS})$$

To evaluate the effectiveness factor for a first-order, isobaric, nonisothermal, flat plate catalyst pellet, the material and energy balances must be solved simultaneously. As shown previously, the mole balance in a slab is given by:

$$\frac{dN_A}{dx} = -k(T) \cdot C_A \tag{6.3.83}$$

where the rate constant is of the Arrhenius form:

$$k(T) = \overline{A} \exp\left(\frac{-E}{R_g T}\right) \tag{6.3.84}$$

The flux of A can be written in terms of Fick's Law:

$$N_A = -D_{TA}^e \frac{dC_A}{dx} \tag{6.3.85}$$

and substituted into the mole balance to give:

$$D_{TA}^e \frac{d^2 C_A}{dx^2} = k(T) \cdot C_A \tag{6.3.86}$$

The energy balance is written in the same manner as the mole balance to give:

$$-\frac{dq}{dx} = (-\Delta H_r) \cdot k(T) \cdot C_A \tag{6.3.87}$$

where the flux is expressed in terms of the effective thermal conductivity of the fluid-solid system, λ^e, and the gradient in temperature:

$$q = -\lambda^e \frac{dT}{dx} \tag{6.3.88}$$

The heat of reaction, ΔH_r, is defined to be negative for exothermic reactions and positive for endothermic reactions. Substitution of Equation (6.3.88) into (6.3.87) results in:

$$\lambda^e \frac{d^2 T}{dx^2} = (-\Delta H_r) \cdot k(T) \cdot C_A \tag{6.3.89}$$

To render the material and energy balances dimensionless, let:

$$\chi = \frac{x}{x_p} \tag{6.3.90}$$

$$\psi = \frac{C_A}{C_{AS}} \tag{6.3.91}$$

$$\Gamma = \frac{T}{T_S} \tag{6.3.92}$$

The rate constant $k(T)$ is expressed in terms of T_S by first forming the ratio:

$$\frac{k(T)}{k(T_S)} = \exp\left[-\frac{E}{R_g}\left(\frac{1}{T} - \frac{1}{T_S}\right)\right] = \exp\left[-\gamma\left(\frac{1}{\Gamma} - 1\right)\right] \tag{6.3.93}$$

where:

$$\gamma = \frac{E}{R_g T_S} \tag{6.3.94}$$

The dimensionless group γ is known as the *Arrhenius* number. Substitution of the dimensionless variables into the material and energy balances gives:

$$\frac{d^2\psi}{d\chi^2} = \left[\frac{(x_p)^2 \cdot k(T_S)}{D_{TA}^e}\right] \cdot \exp\left[-\gamma\left(\frac{1}{\Gamma} - 1\right)\right] \cdot \psi \tag{6.3.95}$$

$$\frac{d^2\Gamma}{d\chi^2} = -\left[\frac{(x_p)^2 \cdot k(T_S) \cdot (-\Delta H_r) \cdot C_{AS}}{\lambda^e T_S}\right] \cdot \exp\left[-\gamma\left(\frac{1}{\Gamma} - 1\right)\right] \cdot \psi \tag{6.3.96}$$

Both equations can be expressed in terms of the Thiele modulus, ϕ, according to:

$$\frac{d^2\psi}{d\chi^2} = \phi^2 \cdot \exp\left[-\gamma\left(\frac{1}{\Gamma} - 1\right)\right] \cdot \psi \tag{6.3.97}$$

$$\frac{d^2\Gamma}{d\chi^2} = -\phi^2\left[\frac{(-\Delta H_r) \cdot D_{TA}^e \cdot C_{AS}}{\lambda^e T_S}\right] \cdot \exp\left[-\gamma\left(\frac{1}{\Gamma} - 1\right)\right] \cdot \psi \tag{6.3.98}$$

A new dimensionless grouping called the *Prater* number, β, appears in the energy balance:

$$\beta = \frac{(-\Delta H_r) \cdot D_{TA}^e \cdot C_{AS}}{\lambda^e T_S} \tag{6.3.99}$$

Thus, the energy balance is rewritten:

$$\frac{d^2\Gamma}{d\chi^2} = -\phi^2 \cdot \beta \cdot \exp\left[-\gamma\left(\frac{1}{\Gamma} - 1\right)\right] \cdot \psi \tag{6.3.100}$$

The material and energy balances are then solved simultaneously with the following boundary conditions:

$$\frac{d\psi}{d\chi} = \frac{d\Gamma}{d\chi} = 0 \qquad \text{at } \chi = 0 \tag{6.3.101}$$

$$\psi = \Gamma = 1 \qquad \text{at } \chi = 1 \tag{6.3.102}$$

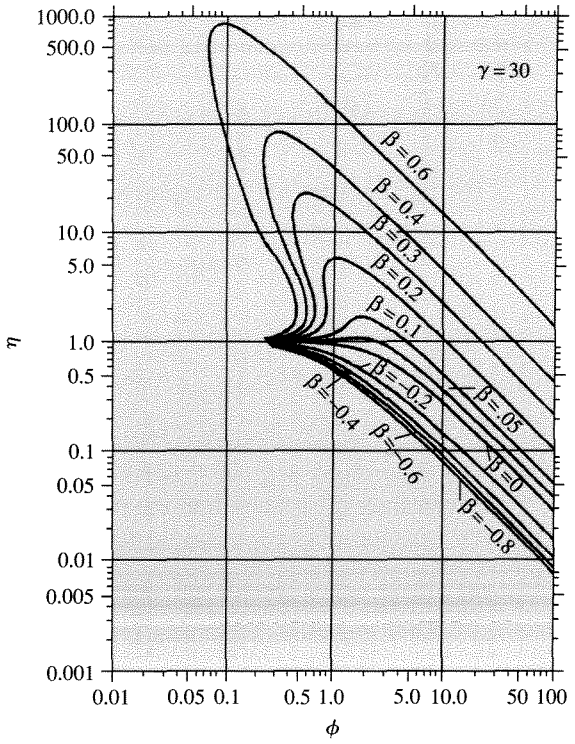

Figure 6.3.12 |
Effectiveness factors for a first-order reaction in a spherical, nonisothermal catalysts pellet. (Reprinted from P. B. Weisz and J. S. Hicks, "The Behavior of Porous Catalyst Particles in View of Internal Mass and Heat Diffusion Effects," *Chem. Eng. Sci.*, **17** (1962) 265, copyright 1962, with permission from Elsevier Science.)

Since the equations are nonlinear, a numerical solution method is required. Weisz and Hicks calculated the effectiveness factor for a first-order reaction in a spherical catalyst pellet as a function of the Thiele modulus for various values of the Prater number [P. B. Weisz and J. S. Hicks, *Chem. Eng. Sci.*, **17** (1962) 265]. Figure 6.3.12 summarizes the results for an Arrhenius number equal to 30. Since the Arrhenius number is directly proportional to the activation energy, a higher value of γ corresponds to a greater sensitivity to temperature. The most important conclusion to draw from Figure 6.3.12 is that effectiveness factors for exothermic reactions (positive values of β) can exceed unity, depending on the characteristics of the pellet and the reaction. In the narrow range of the Thiele modulus between about 0.1 and 1, three different values of the effectiveness factor can be found (but only two represent stable steady states). The ultimate reaction rate that is achieved in the pellet

depends on how the reaction is initiated. Effectiveness factors associated with the negative values of β on Figure 6.3.12 are all less than one, which is expected for endothermic reactions.

It is often useful to quickly estimate the maximum possible temperature rise, also known as the adiabatic temperature rise, in a catalyst pellet. Since no heat is transferred to the surroundings in this case, all energy generated (or consumed) by the reaction goes to heat (or cool) the pellet. The temperature difference between the surface and the pellet interior is directly related to the concentration difference. Dividing the material balance by the energy balance eliminates the reaction rate:

$$\frac{\left[\dfrac{d^2\psi}{d\chi^2}\right]}{\left[\dfrac{d^2\Gamma}{d\chi^2}\right]} = -\frac{1}{\beta} \tag{6.3.103}$$

$$d^2\Gamma = -\beta \cdot d^2\psi \tag{6.3.104}$$

Integrating once gives:

$$d\Gamma = -\beta \cdot d\psi + \bar{\alpha}_1 \tag{6.3.105}$$

The constant $\bar{\alpha}_1$ is evaluated by using the condition at the center of the pellet:

$$d\Gamma = d\psi = 0 \qquad \text{at } \chi = 0$$

$$\bar{\alpha}_1 = 0 \tag{6.3.106}$$

Integrating a second time gives:

$$\Gamma = -\beta \cdot \psi + \bar{\alpha}_2 \tag{6.3.107}$$

The constant $\bar{\alpha}_2$ is found by using the condition at the surface of the pellet:

$$\Gamma = \psi = 1 \qquad \text{at } \chi = 1$$

and

$$\bar{\alpha}_2 = 1 + \beta \tag{6.3.108}$$

Therefore, the relationship between temperature and concentration is:

$$\Gamma = 1 + \beta(1 - \psi)$$

$$\frac{T}{T_S} = 1 + \left[\frac{(-\Delta H_r)D_{TA}^e C_{AS}}{\lambda^e T_S}\right]\left(1 - \frac{C_A}{C_{AS}}\right)$$

$$T = T_S + \left[\frac{(-\Delta H_r)D_{TA}^e}{\lambda^e}\right](C_{AS} - C_A) \tag{6.3.109}$$

Equation (6.3.109) is called the *Prater* relation. From this relationship, the adiabatic temperature rise in a catalyst pellet can be calculated. The maximum

temperature is reached when the reactant is completely converted in the pellet, that is, $C_A = 0$:

$$T_{\max} - T_S = \frac{(-\Delta H_r) D_{TA}^e C_{AS}}{\lambda^e} \tag{6.3.110}$$

$$\frac{T_{\max} - T_S}{T_S} = \frac{(-\Delta H_r) D_{TA}^e C_{AS}}{\lambda^e T_S} \tag{6.3.111}$$

Notice that the dimensionless maximum temperature rise in the catalyst pellet is simply the Prater number β:

$$\frac{T_{\max} - T_S}{T_S} = \beta$$

6.4 | Combined Internal and External Transport Effects

The previous two sections describe separately the significant role that diffusion through a stagnant film surrounding a catalyst pellet and transport through the catalyst pores can play in a solid-catalyzed chemical reaction. However, these two diffusional resistances must be evaluated simultaneously in order to properly interpret the observed rate of a catalytic reaction.

VIGNETTE 6.4.1

Kehoe and Butt studied the hydrogenation of benzene over a solid catalyst consisting of 58 wt. % Ni metal particles supported on kieselguhr powder [J. P. G. Kehoe and J. B. Butt, *AIChE J.*, **18** (1972) 347]. The catalyst had a surface area of 150 $m^2\ g^{-1}$ and an average pore radius of 3.7 nm. This powder was compressed into a cylindrical pellet (1.3 cm diameter by 5.8 cm height) large enough to incorporate four thermocouples along the radial direction. A second pellet was prepared by diluting the original Ni catalyst powder with alumina and graphite in order to increase the thermal conductivity of the catalyst by one order of magnitude. Figure 6.4.1 shows the temperature profile through the film and the catalyst for both pellets exposed to the same feed conditions and run at the same reaction rate. The undiluted catalyst pellet (upper figure) had a measurable intraparticle temperature gradient. Indeed, the center of the pellet was almost 30 K hotter than the external surface, whereas the temperature change over the external film was less than 10 K. The effectiveness factor for this pellet (1.9) was significantly greater than unity because the pellet was hotter than the surrounding bulk fluid. The temperature profile in the second pellet was virtually flat throughout the entire pellet because of its high thermal conductivity (Figure 6.4.1). The only significant temperature gradient for the second pellet was measured across the film. Since the second pellet was operating at a temperature higher than the bulk fluid, the effectiveness factor (1.2) also exceeded unity. However, it was not as high as that encountered with the first pellet because of its lower operating temperature.

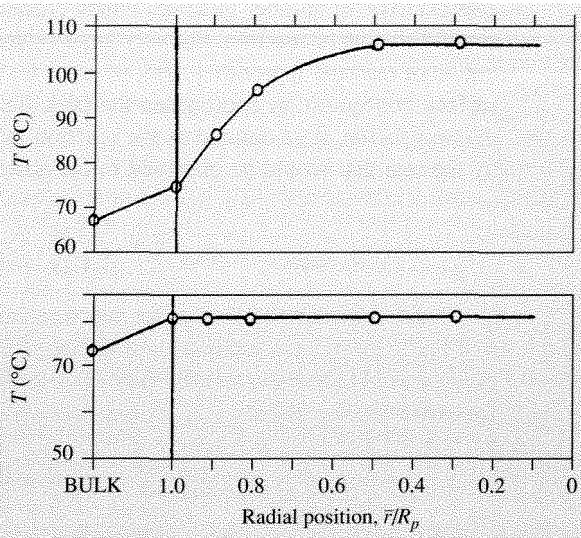

Figure 6.4.1 | Measured external and internal temperature profiles for undiluted Ni catalyst (upper figure) and Ni catalyst diluted in alumina and graphite (lower figure). Feed conditions: 14% C_6H_6, 86% H_2, T_{feed} = 338–340 K, P = 1 atm, H_2 flow 9.0($\pm$1.2) $\times 10^{-3}$ mol s^{-1}. Measured rate: 2.44 $\pm$ 0.08 $\times 10^{-6}$ mol s^{-1} $gcat^{-1}$. (Adapted from J. P. G. Kehoe and J. B. Butt, *AIChE J.*, **18** (1972) 347, with permission of the American Institute of Chemical Engineers. Copyright © 1972 AIChE. All rights reserved.)

Consider a first-order reaction occurring on a *nonporous* flat plate catalyst pellet. In Section 6.2, it was shown that the concentration of reactant A on the external surface of the catalyst is related to both the mass transfer coefficient, $\bar{k}_c$, and the surface rate constant, k_S:

$$C_{AS} = \frac{\bar{k}_c C_{AB}}{k_S + \bar{k}_c} \tag{6.4.1}$$

A dimensionless parameter Da, called the *Damkohler* number, is defined to be the ratio of k_S and $\bar{k}_c$:

$$Da = \frac{k_S}{\bar{k}_c} \tag{6.4.2}$$

so that the surface concentration can be written as:

$$C_{AS} = \frac{C_{AB}}{1 + Da} \tag{6.4.3}$$

The Damkohler number indicates which characteristic first-order process is faster, external diffusion or reaction. For very large values of Da ($k_S >> \bar{k}_c$), the surface concentration of reactant approaches zero, whereas for very small values of Da ($k_S << \bar{k}_c$), the surface concentration approaches the bulk fluid concentration. An *interphase effectiveness factor*, $\bar{\eta}$, is defined as the reaction rate based on surface conditions divided by the rate that would be observed in the absence of diffusional limitations:

$$\bar{\eta} = \frac{k_S C_{AS}}{k_S C_{AB}} = \frac{1}{1 + Da} \tag{6.4.4}$$

Now consider the first-order reaction in a porous flat plate catalyst pellet so that both external (interphase) and internal (intraphase) transport limitations are encountered. At steady state, the flux of A to the surface of the pellet is equal to the flux entering the pellet:

$$\bar{k}_c\left(C_{AS} - C_{AB}\right) = -D^e_{TA}\left.\frac{dC_A}{dx}\right|_S \tag{6.4.5}$$

The energy balance is completely analogous:

$$h_t(T_S - T_B) = -\lambda^e\left.\frac{dT}{dx}\right|_S \tag{6.4.6}$$

Rewriting these two equations in dimensionless form, using the usual substitution for distance:

$$\chi = \frac{x}{x_p} \tag{6.4.7}$$

yields:

$$\left.\frac{d\left(\frac{C_A}{C_{AB}}\right)}{d\chi}\right|_{\chi=1} = Bi_m\left[1 - \frac{C_{AS}}{C_{AB}}\right] \tag{6.4.8}$$

$$\left.\frac{d\left(\frac{T}{T_B}\right)}{d\chi}\right|_{\chi=1} = Bi_h\left[1 - \frac{T_S}{T_B}\right] \tag{6.4.9}$$

where:

$$Bi_m = \frac{x_p \bar{k}_c}{D^e_{TA}} \qquad \text{Biot number for mass} \tag{6.4.10}$$

$$Bi_h = \frac{x_p h_t}{\lambda^e} \qquad \text{Biot number for heat} \tag{6.4.11}$$

Since the concentration and temperature variables in Equations (6.4.8) and (6.4.9) are grouped with their respective bulk fluid values, new dimensionless parameters

need to be defined. Let:

$$\Psi = \frac{C_A}{C_{AB}} \tag{6.4.12}$$

$$\overline{\Gamma} = \frac{T}{T_B} \tag{6.4.13}$$

The dimensionless material and energy balances, with associated boundary conditions, must be solved simultaneously to get the concentration and temperature profiles through the stagnant film and into the catalyst particle. Those relationships are given below:

$$\frac{d^2\Psi}{d\chi^2} = \phi^2\Psi \exp\left[-\gamma\left(\frac{1}{\overline{\Gamma}} - 1\right)\right] \tag{6.4.14}$$

$$\frac{d^2\overline{\Gamma}}{d\chi^2} = -\beta\phi^2\Psi \exp\left[-\gamma\left(\frac{1}{\overline{\Gamma}} - 1\right)\right] \tag{6.4.15}$$

where:

$$\phi^2 = \frac{(x_p)^2 \cdot k(T_B)}{D^e_{TA}} \qquad \beta = \frac{(-\Delta H_r)D^e_{TA}C_{AB}}{\lambda^e T_B} \qquad \gamma = \frac{E}{R_g T_B}$$

Notice that all of the parameters are based on bulk fluid values of the concentration and temperature. The boundary conditions are:

$$\frac{d\Psi}{d\chi} = \frac{d\overline{\Gamma}}{d\chi} = 0 \qquad \text{at } \chi = 0 \tag{6.4.16}$$

$$\frac{d\Psi}{d\chi} = Bi_m(1 - \Psi) \qquad \text{at } \chi = 1 \tag{6.4.17}$$

$$\frac{d\overline{\Gamma}}{d\chi} = Bi_h(1 - \overline{\Gamma}) \qquad \text{at } \chi = 1 \tag{6.4.18}$$

In general, solution of these equations requires a numerical approach.

EXAMPLE 6.4.1

Find an expression for the *overall* effectiveness factor of a first-order *isothermal* reaction in a flat plate catalyst pellet.

■ Answer

Since the reaction is isothermal, the energy balance can be ignored and the mass balance reduces to:

$$\frac{d^2\Psi}{d\chi^2} = \phi^2\Psi \tag{6.4.19}$$

with boundary conditions:

$$\frac{d\Psi}{d\chi} = 0 \qquad \text{at } \chi = 0 \tag{6.4.20}$$

$$\frac{d\Psi}{d\chi} = Bi_m(1 - \Psi) \qquad \text{at } \chi = 1 \tag{6.4.21}$$

As discussed previously, the general solution of the differential equation is:

$$\Psi = \bar{\alpha}_1 \exp(\phi\chi) + \bar{\alpha}_2 \exp(-\phi\chi) \tag{6.4.22}$$

The constants are evaluated by using the appropriate boundary conditions. At the center of the pellet:

$$\left.\frac{d\Psi}{d\chi}\right|_{\chi=0} = 0 = \bar{\alpha}_1 \phi \exp\left(\phi \cdot 0\right) - \bar{\alpha}_2 \phi \exp\left(-\phi \cdot 0\right) \tag{6.4.23}$$

$$\bar{\alpha}_1 = \bar{\alpha}_2 \tag{6.4.24}$$

Substitution of Equation (6.4.24) into (6.4.22) eliminates one of the integration constants:

$$\Psi = \bar{\alpha}_1 \exp(\phi\chi) + \bar{\alpha}_1 \exp(-\phi\chi) \tag{6.4.25}$$

$$\Psi = 2\bar{\alpha}_1 \frac{\exp(\phi\chi) + \exp(-\phi\chi)}{2} \tag{6.4.26}$$

$$\Psi = 2\bar{\alpha}_1 \cosh(\phi\chi) \tag{6.4.27}$$

$$\frac{d\Psi}{d\chi} = 2\bar{\alpha}_1 \phi \sinh(\phi\chi) \tag{6.4.28}$$

The boundary condition at the external surface provides another relation for $d\Psi/d\chi$:

$$\left.\frac{d\Psi}{d\chi}\right|_{\chi=1} = Bi_m[1 - \Psi] = Bi_m[1 - 2\bar{\alpha}_1 \cosh(\phi)] \tag{6.4.29}$$

Equating Equations (6.4.28) and (6.4.29), at $\chi = 1$, enables the determination of $\bar{\alpha}_1$:

$$2\bar{\alpha}_1 \phi \sinh(\phi) = Bi_m[1 - 2\bar{\alpha}_1 \cosh(\phi)] \tag{6.4.30}$$

$$\bar{\alpha}_1 = \frac{Bi_m}{2[\phi \sinh(\phi) + Bi_m \cosh(\phi)]} \tag{6.4.31}$$

and therefore,

$$\Psi = \frac{Bi_m \cosh(\phi\chi)}{\phi \sinh(\phi) + Bi_m \cosh(\phi)} \tag{6.4.32}$$

Since the concentration profile is determined by Equation (6.4.32), evaluation of the *overall effectiveness factor*, η_o, is straightforward. By definition, η_o is the observed rate divided by the rate that would be observed at conditions found in the bulk fluid. Recall

that the observed rate must equal the flux of A at the surface of the pellet at the steady state:

$$\eta_o = \frac{r_{obs}}{r_{max}} = \frac{(Area)D_{TA}^e \left.\frac{dC_A}{dx}\right|_{x=x_p}}{(Area)x_p k C_{AB}} = \frac{\left.\frac{d\Psi}{d\chi}\right|_{\chi=1}}{\phi^2} \tag{6.4.33}$$

$$\eta_o = \frac{\tanh(\phi)}{\phi\left[1 + \frac{\phi\tanh(\phi)}{Bi_m}\right]} \tag{6.4.34}$$

The overall effectiveness factor is actually comprised of the individual effectiveness factors for intraphase and interphase transport:

$$\eta_o = \eta_{\text{intraphase}} \cdot \eta_{\text{interphase}} = \eta \cdot \overline{\eta} \tag{6.4.35}$$

For example, an isothermal, first-order reaction in a flat plate catalyst pellet has individual effectiveness factors that are:

$$\eta = \frac{\tanh(\phi)}{\phi} \tag{6.4.36}$$

$$\overline{\eta} = \left[1 + \frac{\phi\tanh(\phi)}{Bi_m}\right]^{-1} \tag{6.4.37}$$

Common ranges of diffusivities, thermal conductivities, mass transfer coefficients, heat transfer coefficients, and catalyst pore sizes can be used to estimate the relative magnitude of artifacts in kinetic data obtained in industrial reactors. For gas-solid heterogeneous systems, the high thermal conductivity of solids compared to gases suggests that the temperature gradient in the film surrounding the catalyst particle is likely to be greater than the temperature gradient in the particle. Since the Knudsen diffusivity of gaseous molecules in a small pore of a catalyst particle is much lower than the molecular diffusivity in the stagnant film, intraphase gradients in mass are likely to be much greater than interphase gradients. For liquid-solid heterogeneous systems, internal temperature gradients are often encountered. A typical range of Bi_m/Bi_h is from 10 to 10^4 for gas-solid systems and from 10^{-4} to 10^{-1} for liquid solid systems.

VIGNETTE 6.4.2

One important process in the manufacturing of electronic materials and devices involves the deposition of thin films onto patterned surfaces. As feature sizes of silicon-based devices continue to shrink in order to increase memory capacity, deposition of uniform films onto surfaces with micron-scale trenches is required. One such film-growth process is called *chemical vapor deposition* (CVD) that involves the reaction of a vapor phase

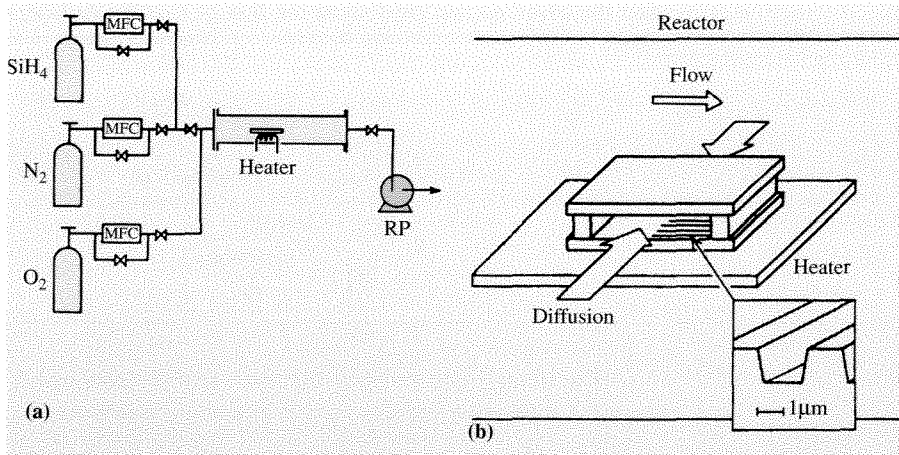

Figure 6.4.2 | **(a)** Schematic diagram of CVD apparatus. MFC and RP represent a mass flow controller and a rotary pump, respectively. **(b)** Schematic structure of the macrocavity reactor consisting of two silicon wafers, each patterned with microcavity trenches. (Reproduced from K. Watanabe and H. Komiyama, "Micro/Macrocavity Method Applied to the Study of the Step Coverage Formation Mechanism of SiO_2 Films by LPCVD," *J. Electrochem. Soc.*, **137** (1990) 1222, with permission of the Electrochemical Society, Inc.)

reactant with a surface. The deposition of reacting species on silicon wafers and in micron-sized trenches involves a balance between diffusion of reactants to the surface and the kinetics of surface deposition reactions. Watanabe and Komiyama analyzed the simultaneous diffusion/reaction phenomena involved with CVD of SiO_2 thin films by reaction of SiH_4 and O_2 [K. Watanabe and H. Komiyama, *J. Electrochem. Soc.*, **137** (1990) 1222]. Figures 6.4.2 (a) and (b) illustrate the CVD system used to study the deposition process. Micron-scale trenches were etched into silicon wafers by normal lithographic procedures. Two wafers were attached to each other with spacers between them, as illustrated in Figure 6.4.2(b). The openings between the two wafers were oriented parallel to the direction of flow. Thus, the reactor configuration has two regions that require diffusive transport of reactants, the macrocavity between the two wafers and the micron-sized trenches (microcavities) on each wafer.

The depth profile of SiO_2 film deposited in a macrocavity of width 0.55 mm at 673 K after 120 min of reaction is shown in Figure 6.4.3. The thickness of the film is greatest at the two open ends of the macrocavity and then rapidly decreases towards the center, presumably because of depletion of reactive species in the macrocavity interior.

Analysis of this system is rather straightforward since it is mathematically equivalent to a catalyst pellet in which reaction and diffusion occur simultaneously. The rate of reaction in this case is simply the growth rate of the film. The collision frequency of gas-phase molecules of A with the surface is given by gas kinetic theory as $(V_A/4)C_A$, where V_A = mean velocity of the gas phase A molecules $(\sqrt{8\bar{k}T/[\pi(M_A)]})$ and M_A is the

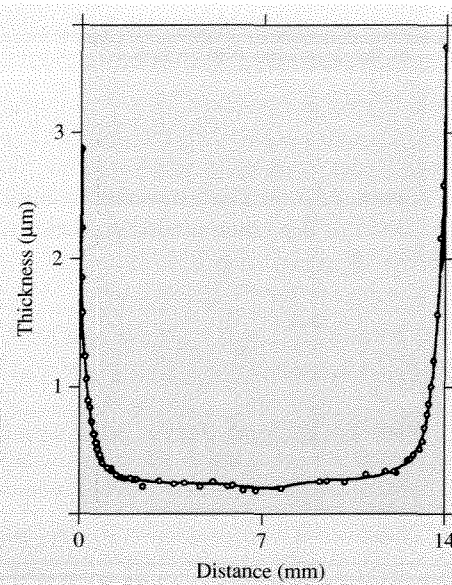

Figure 6.4.3 | Growth rate profile of SiO_2 in the macrocavity. (Reproduced from K. Watanabe and H. Komiyama, "Micro/Macrocavity Method Applied to the Study of the Step Coverage Formation Mechanism of SiO_2 Films by LPCVD," *J. Electrochem. Soc.*, **137** (1990) 1222, with permission of the Electrochemical Society, Inc.)

molecular weight of A. Thus, the growth rate of the film is simply the fraction of molecules that stick to the surface, sticking coefficient S_c, times the overall collision rate with the surface, $S_c(V_A/4)C_A$. The material balance on the macrocavity is analogous to Equation (6.3.10) and is:

$$\frac{d^2C_A}{dx^2} - \frac{S_c\left(\frac{V_A}{4}\right)}{D_{TA}\left(\frac{W_c}{2}\right)} C_A = 0 \tag{6.4.38}$$

where W_c is the width of the macrocavity. Solving Equation (6.4.38) with the following boundary conditions:

$$C_A = C_A^0 \qquad \text{at } x = 0$$

$$\frac{dC_A}{dx} = 0 \qquad \text{at } x = L_c \quad (\text{where } L_c \text{ is the half length of the macrocavity})$$

gives an analytical expression for C_A throughout the macrocavity and thus the growth rate of the deposited film, which is:

$$\text{Growth Rate} = S_c\left(\frac{V_A}{4}\right)C_A^0\left(\frac{\cosh[\phi'(L_c - x)/L_c]}{\cosh(\phi')}\right) \tag{6.4.39}$$

where ϕ' is the Thiele modulus. In this case, the Thiele modulus is the ratio of the characteristic deposition rate to the characteristic diffusion rate according to:

$$\phi' = L_c\sqrt{\frac{S_c\left(\frac{V_A}{4}\right)}{D_{TA}\left(\frac{W_c}{2}\right)}} \tag{6.4.40}$$

The growth rate profiles predicted by Equation (6.4.39) are given in Figure 6.4.4.

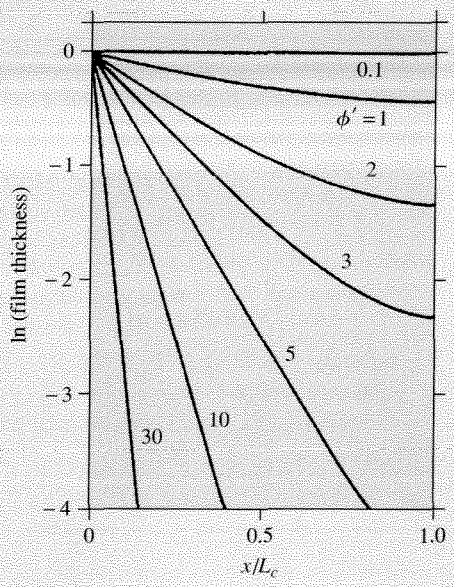

Figure 6.4.4 | Growth rate profiles in the macrocavity reactor predicted by Equation 6.4.39. Film thickness is normalized by the value at inlet of the cavity. (Adapted from K. Watanabe and H. Komiyama, "Micro/Macrocavity Method Applied to the Study of the Step Coverage Formation Mechanism of SiO_2 Films by LPCVD," *J. Electrochem. Soc.*, **137** (1990) 1222, with permission of the Electrochemical Society, Inc.)

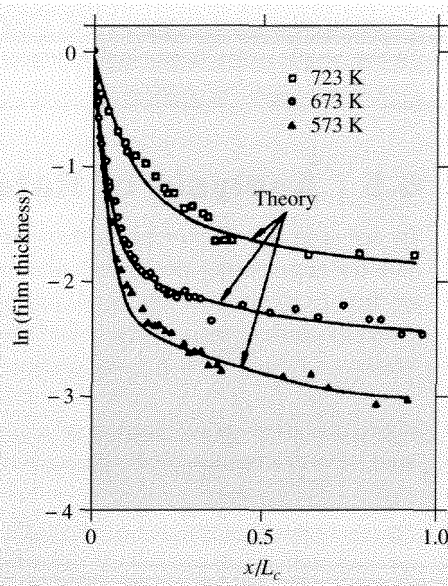

Figure 6.4.5 | Growth rate profiles obtained in the macrocavity reactor at various temperatures. Solid curves were obtained from the model containing gas-phase reaction and deposition on the surface. Film thickness is normalized by value at inlet of the cavity. (Adapted from K. Watanabe and H. Komiyama, "Micro/Macrocavity Method Applied to the Study of the Step Coverage Formation Mechanism of SiO_2 Films by LPCVD," *J. Electrochem. Soc.*, **137** (1990) 1222, with permission of the Electrochemical Society, Inc.)

Although the curves in Figure 6.4.4 represent the essential features of the simultaneous reaction/diffusion phenomena that occur in CVD processing, they do not reproduce the measured film thickness throughout the entire reactor as given in Figure 6.4.3. Watanabe and Komiyama derived a slightly more complex reaction/diffusion model in which the SiH_4 reacts in the gas phase to form a very dilute reactive intermediate which then deposits onto the wafer as SiO_2. This new model incorporates diffusion, gas-phase reaction, and surface deposition and fits the experimental data very well at three different temperatures, as illustrated in Figure 6.4.5.

Deposition of SiO_2 in the micron-sized trenches is also dependent on simultaneous diffusion and reaction. Watanabe and Komiyama found that the growth rate of the film at 573–723 K on the bottom of 1.2 μm deep trenches was less than that on the surface for

trench widths less than about 3 μm. Clearly, solution of reaction/diffusion equations over many length scales is required to model the deposition of thin films during CVD processing of electronic materials.

6.5 | Analysis of Rate Data

To arrive at a rate expression that describes intrinsic reaction kinetics and is suitable for engineering design calculations, one must be assured that the kinetic data are free from artifacts that mask intrinsic rates. A variety of criteria have been proposed to guide kinetic analysis and these are thoroughly discussed by Mears [D. E. Mears, *Ind. Eng. Chem. Process Des. Develop.*, **10** (1971) 541].

A lack of significant intraphase diffusion effects (i.e., $\eta \geq 0.95$) on an irreversible, isothermal, first-order reaction in a spherical catalyst pellet can be assessed by the Weisz-Prater criterion [P. B. Weisz and C. D. Prater, *Adv. Catal.*, **6** (1954) 143]:

$$\frac{\mathrm{r}_{\mathrm{obs}}\,(R_p)^2}{D^e_{TA}C_{AS}} < 1 \tag{6.5.1}$$

where $\mathrm{r}_{\mathrm{obs}}$ is the observed reaction rate per unit volume and R_p is the radius of a catalyst particle. An important aspect of this criterion is that it uses the *observed* rate and the reactant concentration at the *external* surface. The intrinsic rate and the concentration profile inside the pellet are not needed. For power law kinetics where n is the reaction order (other than 0), the following expression can be used:

$$\frac{\mathrm{r}_{\mathrm{obs}}\,(R_p)^2}{D^e_{TA}C_{AS}} < \frac{1}{\mathrm{n}} \tag{6.5.2}$$

The influence of mass transfer through the film surrounding a spherical catalyst particle can also be examined with a similar expression. Satisfaction of the following inequality demonstrates that interphase mass transfer is not significantly affecting the measured rate:

$$\frac{\mathrm{r}_{\mathrm{obs}}R_p}{\bar{k}_c C_{AB}} < \frac{0.15}{n} \tag{6.5.3}$$

where $\bar{k}_c$ is the mass transfer coefficient and the reactant concentration is determined in bulk fluid. The above relationship is analogous to the modified Weisz-Prater criterion with $\bar{k}_c$ replacing D^e_{TA}/R_p.

Criteria have also been developed for evaluating the importance of intraphase and interphase heat transfer on a catalytic reaction. The Anderson criterion for estimating the significance of intraphase temperature gradients is [J. B. Anderson, *Chem. Eng. Sci.*, **18** (1963) 147]:

$$\frac{|\Delta H_r|\mathrm{r}_{\mathrm{obs}}\,(R_p)^2}{\lambda^e T_S} < 0.75\frac{R_g T_S}{E} \tag{6.5.4}$$

where λ^e is the effective thermal conductivity of the particle and E is the true activation energy. Satisfying the above criterion guarantees that r_{obs} does not differ from the rate at constant temperature by more than 5 percent. Equation (6.5.4) is valid whether or not diffusional limitations exist in the catalyst particle. An analogous criterion for the lack of interphase temperature gradients has been proposed by Mears [D. E. Mears, *J. Catal.*, **20** (1971) 127]:

$$\frac{|\Delta H_r| r_{obs} R_p}{h_t T_B} < 0.15 \frac{R_g T_B}{E} \tag{6.5.5}$$

where h_t is the heat transfer coefficient and T_B refers to the bulk fluid temperature. The Mears criterion is similar to the Anderson criterion with h_t replacing λ^e/R_p. In addition, the Mears criterion is also valid in the presence of transport limitations in the catalyst particle.

While the above criteria are useful for diagnosing the effects of transport limitations on reaction rates of heterogeneous catalytic reactions, they require knowledge of many physical characteristics of the reacting system. Experimental properties like effective diffusivity in catalyst pores, heat and mass transfer coefficients at the fluid-particle interface, and the thermal conductivity of the catalyst are needed to utilize Equations (6.5.1) through (6.5.5). However, it is difficult to obtain accurate values of those critical parameters. For example, the diffusional characteristics of a catalyst may vary throughout a pellet because of the compression procedures used to form the final catalyst pellets. The accuracy of the heat transfer coefficient obtained from known correlations is also questionable because of the low flow rates and small particle sizes typically used in laboratory packed bed reactors.

Madon and Boudart propose a simple experimental criterion for the absence of artifacts in the measurement of rates of heterogeneous catalytic reactions [R. J. Madon and M. Boudart, *Ind. Eng. Chem. Fundam.*, **21** (1982) 438]. The experiment involves making rate measurements on catalysts in which the concentration of active material has been purposely changed. In the absence of artifacts from transport limitations, the reaction rate is directly proportional to the concentration of active material. In other words, the intrinsic turnover frequency should be independent of the concentration of active material in a catalyst. One way of varying the concentration of active material in a catalyst pellet is to mix inert particles together with active catalyst particles and then pelletize the mixture. Of course, the diffusional characteristics of the inert particles must be the same as the catalyst particles, and the initial particles in the mixture must be much smaller than the final pellet size. If the diluted catalyst pellets contain 50 percent inert powder, then the observed reaction rate should be 50 percent of the rate observed over the undiluted pellets. An intriguing aspect of this experiment is that measurement of the number of active catalytic sites is not involved with this test. However, care should be exercised when the dilution method is used with catalysts having a bimodal pore size distribution. Internal diffusion in the micropores may be important for both the diluted and undiluted catalysts.

Another way to change concentration of active material is to modify the catalyst loading on an inert support. For example, the number of supported transition metal particles on a microporous support like alumina or silica can easily be varied during catalyst preparation. As discussed in the previous chapter, selective chemisorption of small molecules like dihydrogen, dioxygen, or carbon monoxide can be used to measure the fraction of exposed metal atoms, or dispersion. If the turnover frequency is independent of metal loading on catalysts with identical metal dispersion, then the observed rate is free of artifacts from transport limitations. The metal particles on the support need to be the same size on the different catalysts to ensure that any observed differences in rate are attributable to transport phenomena instead of structure sensitivity of the reaction.

A minor complication arises when dealing with *exothermic* reactions, since the effectiveness factor for a catalyst pellet experiencing transport limitations can still equal one. To eliminate any ambiguity associated with this rare condition, the Madon-Boudart criterion for an exothermic reaction should be repeated at a different temperature.

The simplicity and general utility of the Madon-Boudart criterion make it one of the most important experimental tests to confirm that kinetic data are free from artifacts. It can be used for heterogeneous catalytic reactions carried out in batch, continuous stirred tank, and tubular plug flow reactors.

VIGNETTE 6.5.1

A good illustration of the Madon-Boudart criterion is the liquid-phase hydrogenation of cyclohexene to cyclohexane over supported Pt/SiO_2 catalysts that differ in Pt loading by a factor of 4 [R. J. Madon and M. Boudart, *Ind. Eng. Chem. Fundam.*, **21** (1982) 438].

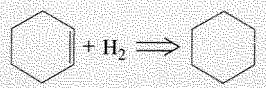

Cyclohexene Cyclohexane

Two catalysts were prepared with 1.5 and 0.38 percent Pt supported on silica. Chemisorption experiments revealed that the percentage of metal exposed was 100 percent on both catalysts. The turnover frequency for liquid-phase cyclohexene hydrogenation (101.3 kPa H_2 pressure) was 2.67 s^{-1} and 2.51 s^{-1} at 275 K and 9.16 and 9.02 at 307 K. The similarity of the turnover frequencies at each of two different temperatures indicates that the measured rates were not influenced by transport limitations.

Development of rate expressions and evaluation of kinetic parameters require rate measurements free from artifacts attributable to transport phenomena. Assuming that experimental conditions are adjusted to meet the above-mentioned criteria for the lack of transport influences on reaction rates, rate data can be used to postulate a kinetic mechanism for a particular catalytic reaction.

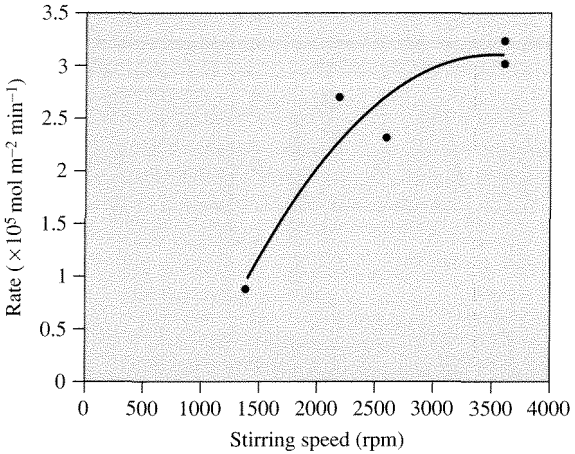

Figure 6.5.1 |
Effect of agitation on the rate of 2-propanol dehydrogenation to acetone at 355 K over Ni catalysts. [Rates are calculated at constant conversion level from the data in D. E. Mears and M. Boudart, *AIChE J.*, **12** (1966) 313.] In this case, increasing the stirring speed increased the rate of acetone diffusion away from the catalyst pellet and decreased product inhibition.

If mass and heat transfer problems are encountered in a catalytic reaction, various strategies are employed to minimize their effects on observed rates. For example, the mass transfer coefficient for diffusion through the stagnant film surrounding a catalyst pellet is directly related to the fluid velocity and the diameter of the pellet according to Equation (6.2.26). When reactions are not mass transfer limited, the observed rate will be independent of process variables that affect the fluid velocity around the catalyst pellets. Conversely, interphase transport limitations are indicated if the observed rate is a function of fluid flow. Consider the results illustrated in Figure 6.5.1 for the dehydrogenation of 2-propanol to acetone over powdered nickel catalyst in a stirred reactor. The dependence of the rate on stirring speed indicates that mass transfer limitations are important for stirring speeds less than 3600 rpm. Additional experiments with different surface area catalysts confirmed that rates measured at the highest stirring speed were essentially free of mass transfer limitations [D. E. Mears and M. Boudart, *AIChE J.*, **12** (1966) 313].

Both interphase and intraphase mass transfer limitations are minimized by decreasing the pellet size of the catalyst. Since a packed bed of very small catalyst particles can cause an unacceptably large pressure drop in a reactor, a compromise between pressure drop and transport limitations is often required in commercial reactors. Fortunately, laboratory reactors that are used to obtain

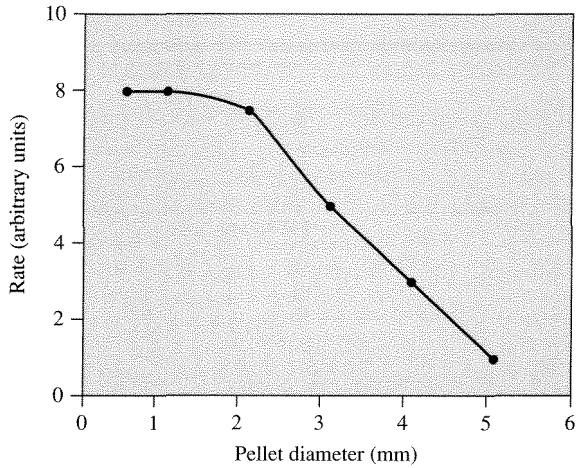

Figure 6.5.2 |
Schematic illustration of the influence of catalyst pellet size on the observed reaction rate.

intrinsic reaction kinetics require relatively small amounts of catalyst and can be loaded with very small particles. For the case presented in Figure 6.5.2, observed rates measured on catalyst pellets larger than 1 mm are affected by transport limitations.

Exercises for Chapter 6

1. The isothermal, first-order reaction of gaseous A occurs within the pores of a spherical catalyst pellet. The reactant concentration halfway between the external surface and the center of the pellet is equal to one-fourth the concentration at the external surface.
   (a) What is the relative concentration of A near the center of the pellet?
   (b) By what fraction should the pellet diameter be reduced to give an effectiveness factor of 0.7?
2. The isothermal, reversible, first-order reaction $A = B$ occurs in a flat plate catalyst pellet. Plot the dimensionless concentration of A (C_A/C_{AS}) as a function of distance into the pellet for various values of the Thiele modulus and the equilibrium constant. To simplify the solution, let $C_{AS} = 0.9(C_A + C_B)$ for all cases.
3. A second-order, irreversible reaction with rate constant $k = 1.8\ \text{L mol}^{-1}\ \text{s}^{-1}$ takes place in a catalyst particle that can be considered to be a one-dimensional slab of half width = 1 cm.

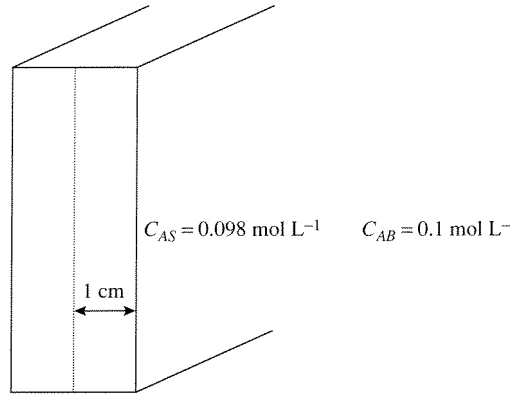

The concentration of reactant in the gas phase is 0.1 mol L^{-1} and at the surface is 0.098 mol L^{-1}. The gas-phase mass-transfer coefficient is 2 cm s^{-1}. Determine the intraphase effectiveness factor. (Contributed by Prof. J. L. Hudson, Univ. of Virginia.)

4. Consider the combustion of a coal particle occurring in a controlled burner. Assume the rate expression of the combustion reaction at the surface of the particle is given by:

$$r = 10^6 \exp[-100/(R_g T_S)]\, C_S \qquad E \text{ in kJ mol}^{-1}$$

where the rate is in units of moles O_2 reacted min^{-1} (m^2 external surface)$^{-1}$, T_S is the surface temperature of the coal particle in Kelvins, and C_S is the surface concentration of O_2. The estimated heat and mass-transfer coefficients from the gas phase to the particle are $h_t = 0.5$ kJ min^{-1} K^{-1} m^{-2} and $\bar{k}_c = 0.5$ m min^{-1}, and the heat of reaction is -150 kJ (mol O_2)$^{-1}$. Consider the bulk temperature of the gas to be $T_B = 500°C$ and the bulk concentration of O_2 to be 2 mol m^{-3}.

(a) What is the maximum temperature difference between the bulk gas and the particle? What is the observed reaction rate under that condition?

(b) Determine the *actual* surface temperature and concentration, and therefore the *actual* reaction rate.

5. The irreversible, first-order reaction of gaseous A to B occurs in spherical catalyst pellets with a radius of 2 mm. For this problem, the molecular diffusivity of A is 1.2×10^{-1} cm^2 s^{-1} and the Knudsen diffusivity is 9×10^{-3} cm^2 s^{-1}. The intrinsic first-order rate constant determined from detailed laboratory measurements was found to be 5.0 s^{-1}. The concentration of A in the surrounding gas is 0.01 mol L^{-1}. Assume the porosity and the tortuosity of the pellets are 0.5 and 4, respectively.

(a) Determine the Thiele modulus for the catalyst pellets.

(b) Find a value for the internal effectiveness factor.

(c) For an external mass-transfer coefficient of 32 s^{-1} (based on the external area of the pellets), determine the concentration of A at the surface of the catalyst pellets.

(d) Find a value for the overall effectiveness factor.

6. J. M. Smith (J. M. Smith, *Chemical Engineering Kinetics,* 2nd ed., McGraw-Hill, New York, 1970, p. 395) presents the following observed data for Pt-catalyzed oxidation of SO_2 at 480°C obtained in a differential fixed-bed reactor at atmospheric pressure and bulk density of 0.8 g/cm^3.

Mass velocity ($g\ h^{-1}\ cm^{-2}$)	Bulk partial pressure (atm)			Observed rate (mol SO_2/h/gcat)
	SO_2	SO_3	O_2	
251	0.06	0.0067	0.2	0.1346
171	0.06	0.0067	0.2	0.1278
119	0.06	0.0067	0.2	0.1215
72	0.06	0.0067	0.2	0.0956

The catalyst pellets were 3.2 by 3.2 mm cylinders, and the Pt was superficially deposited upon the external surface. Compute both external mass and temperature gradients and plot ΔC_{SO_2} and ΔT versus the mass velocity. Can you draw any qualitative conclusions from this plot? If the reaction activation energy is 30 kcal/mol, what error in rate measurement attends neglect of an external ΔT? What error prevails if, assuming linear kinetics in SO_2, external concentration gradients are ignored?

Hints:

$$J = \frac{\bar{k}_c}{u} Sc^{2/3} = 0.817\, Re^{-1/2}$$

catalyst pellet is nonporous

reaction carried out with excess air

$\bar{\mu}_{air} = 1.339$ g/h/cm @ 480°C

$D_{SO_2-air} = 2.44$ ft^2/h @ 480°C

$\bar{\varepsilon}_B$ = void fraction of bed = 0.4

$Sc = 1.28$

$$\text{Prandtl number} = \frac{\bar{\mu}\, C_p}{\lambda} = 0.686$$

$C_p = 7.514$ cal/mol/K

$$a = \frac{\text{surface area}}{\text{volume}} = 18.75\ \text{mm}^{-1}$$

$\Delta H_r = -30$ kcal/mol

7. The importance of diffusion in catalyst pellets can often be determined by measuring the effect of pellet size on the observed reaction rate. In this exercise, consider an irreversible first-order reaction occurring in catalyst pellets where the surface concentration of reactant A is $C_{AS} = 0.15$ M.

   Data:

Diameter of sphere (cm)	0.2	0.06	0.02	0.006
r_{obs} (mol/h/cm^3)	0.25	0.80	1.8	2.5

   (a) Calculate the intrinsic rate constant and the effective diffusivity.

   (b) Estimate the effectiveness factor and the anticipated rate of reaction (r_{obs}) for a finite cylindrical catalyst pellet of dimensions 0.6 cm × 0.6 cm (diameter = length).

8. Isobutylene (A) reacts with water on an acidic catalyst to form t-butanol (B).

$$(CH_3)_2C{=}CH_2 + H_2O = (CH_3)_3COH$$

   When the water concentration greatly exceeds that of isobutylene and t-butanol, the reversible hydration reaction is effectively first order in both the forward and reverse directions.

   V. P. Gupta and W. J. M. Douglas [*AIChE J.*, **13** (1967) 883] carried out the isobutylene hydration reaction with excess water in a stirred tank reactor utilizing a cationic exchange resin as the catalyst. Use the following data to determine the effectiveness factor for the ion exchange resin at 85°C and 3.9 percent conversion.

   Data:

   Equilibrium constant @ 85°C = 16.6 = $[B]/[A]$

   $D^e_{TA} = 2.0 \times 10^{-5}$ cm^2 s^{-1}

   Radius of spherical catalyst particle = 0.213 mm

   Density of catalyst = 1.0 g cm^{-3}

   Rate of reaction at 3.9 percent conversion = 1.11×10^{-5} mol s^{-1} gcat^{-1}

   $C_{AS} = 1.65 \times 10^{-2}$ M (evaluated at 3.9 percent conversion)

   $C^0_A = 1.72 \times 10^{-2}$ M (reactor inlet concentration)

   (Problem adapted from C. G. Hill, Jr., *An Introduction to Chemical Engineering Kinetics and Reactor Design*, Wiley, NY, 1977.)

9. Ercan et al. studied the alkylation of ethylbenzene, *EB*, with light olefins (ethylene and propylene) over a commercial zeolite Y catalyst in a fixed-bed reactor with recycle [C. Ercan, F. M. Dautzenberg, C. Y. Yeh, and H. E. Barner, *Ind. Eng. Chem. Res.*, **37** (1998) 1724]. The solid-catalyzed liquid-phase reaction was carried out in excess ethylbenzene at 25 bar and 190°C. Assume

the reaction is pseudo-first-order with respect to olefin. The porosity of the catalyst was 0.5, the tortuosity was 5.0, and the density was 1000 kg m^{-3}. The observed rate (r_{obs}) and rate constant (k_{obs}) were measured for two different catalyst pellet sizes. Relevant results are given below:

R_p (mm)	$\bar{k}_c$ (m s^{-1})	External surface area of catalyst, S_p (m^2 kg^{-1})	r_{obs} (kmol (kgcat s)$^{-1}$)	k_{obs} (m^3 (kgcat s)$^{-1}$)
0.63	5.69×10^{-4}	4.62	8.64×10^{-6}	0.33×10^{-3}
0.17	1.07×10^{-3}	17.13	11.7×10^{-6}	1.06×10^{-3}

(a) Determine whether or not external and internal mass transfer limitations are significant for each case. Assume the diffusivity of olefins in ethylbenzene is $D_{AB} = 1.9 \times 10^{-4}$ cm^2 s^{-1}.

(b) Calculate the Thiele modulus, ϕ, and the internal effectiveness factor, η, for each case.

(c) Determine the overall effectiveness factor for each case.

10. Reaction rate expressions of the form:

$$r = \frac{kC_A}{1 + KC_A}$$

reveal zero-order kinetics when $KC_A \gg 1$. Solve the material balance (isothermal) equation for a slab catalyst particle using zero-order kinetics. Plot $C_A(x)/C_{AS}$ for a Thiele modulus of 0.1, 1.0, and 10.0. If the zero-order kinetics were to be used as an approximation for the rate form shown above when $KC_{AS} \gg 1$, would this approximation hold with the slab catalyst particle for the Thiele moduli investigated?

11. Kehoe and Butt [J. P. Kehoe and J. B. Butt, *AIChE J.*, **18** (1972) 347] have reported the kinetics of benzene hydrogenation of a supported, partially reduced Ni/kieselguhr catalyst. In the presence of a large excess of hydrogen (90 percent) the reaction is pseudo-first-order at temperatures below 200°C with the rate given by:

$$r = \left(P_H^0 k_1^0 K^0\right) \exp\left[\frac{-E}{R_g T}\right] P_B$$

where

P_B = benzene partial pressure, torr
P_H^0 = dihydrogen partial pressure, torr
$K^0 = 4.22 \times 10^{-11}$ $torr^{-1}$
$k_1^0 = 4.22$ mol/gcat/s/torr
$E = -2.7$ kcal/mol

For the case of $P_H^0 = 685$ torr, $P_B = 75$ torr, and $T = 150°C$, estimate the effectiveness factor for this reaction carried out in a spherical catalyst particle of density 1.88 gcat/cm^3, $D_{TB}^e = 0.052$ cm^2/s, and $R_p = 0.3$ cm.

12. A first-order irreversible reaction is carried out on a catalyst of characteristic dimension 0.2 cm and effective diffusivity of 0.015 cm^2/s. At 100°C the intrinsic rate constant has been measured to be 0.93 s^{-1} with an activation energy of 20 kcal/mol.

(a) For a surface concentration of 3.25×10^{-2} mol/L, what is the observed rate of reaction at 100°C?

(b) For the same reactant concentration, what is the observed rate of reaction at 150°C? Assume that D_{TA}^e is independent of temperature.

(c) What value of the activation energy would be observed?

(d) Compare values of the Thiele modulus at 100°C and 150°C.

13. The catalytic dehydrogenation of cyclohexane to benzene was accomplished in an isothermal, differential, continuous flow reactor containing a supported platinum catalyst [L. G. Barnett et al., *AIChE J.*, **7** (1961) 211].

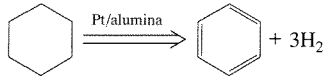

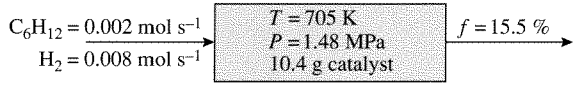

Dihydrogen was fed to the process to minimize deposition of carbonaceous residues on the catalyst. Assuming the reaction is first-order in cyclohexane and the diffusivity is primarily of the Knudsen type, estimate the tortuosity $\bar{\tau}$ of the catalyst pellets.

Additional Data:

Diameter of catalyst pellet = 3.2 mm
Pore volume of the catalyst = 0.48 cm^3 g^{-1}
Surface area = 240 m^2 g^{-1}
Pellet density $\rho_p = 1.332$ g cm^{-3}
Pellet Porosity $\bar{\varepsilon}_p = 0.59$
Effectiveness factor $\eta = 0.42$

14. For a slab with first-order kinetics:

$$\eta_o = \frac{\tanh\phi}{\phi[1 + \phi\tanh(\phi)/Bi_m]} \tag{1}$$

How important is the mass Biot number in Equation (1) with respect to its influence upon η_o for (a) $\phi = 0.1$, (b) $\phi = 1.0$, (c) $\phi = 5.0$, (d) $\phi = 10.0$?

Consider the effect of the Biot number significant if it changes η_o by more than 1 percent. Can you draw any qualitative conclusions from the behavior observed in parts (a)–(d)?

15. The liquid-phase hydrogenation of cyclohexene to cyclohexane (in an inert solvent) is conducted over solid catalyst in a semibatch reactor (dihydrogen addition to keep the total pressure constant).

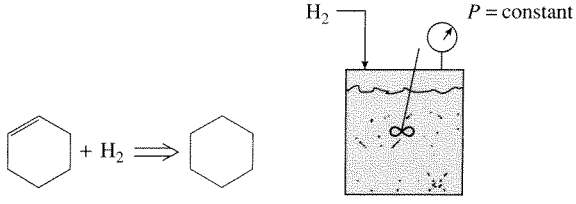

Draw a schematic representation of what is occurring at the microscopic level. Provide an interpretation for each of the following figures.

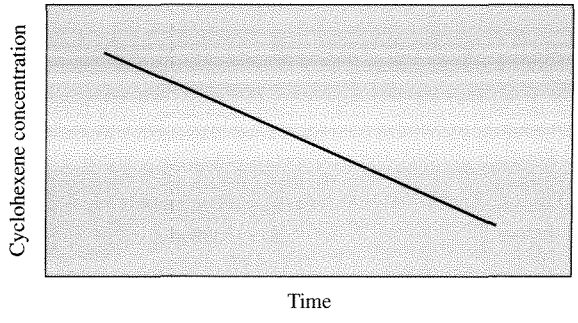

Figure 1 |
Linear relationship between cyclohexene concentration in the reactor and reaction time. Results apply for all conditions given in the figures provided below.

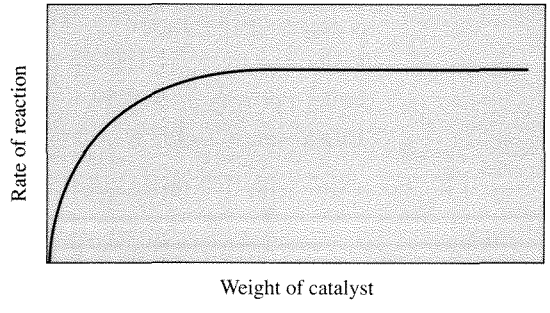

Figure 2 |
Effect of catalyst weight on reaction rate.

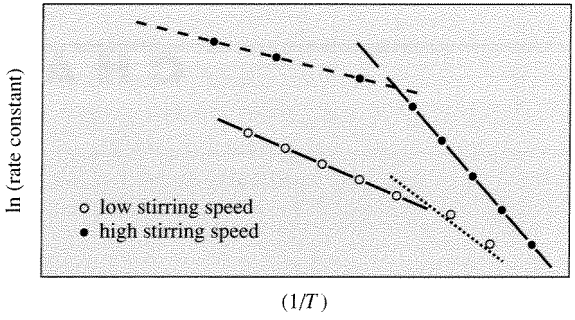

Figure 3 |
Evaluation of temperature effects on the reaction rate constant.